Manuscript #: 2015AUTO0717

INHIBITION OF RETROGRADE TRANSPORT MODULATES MISFOLDED PROTEIN ACCUMULATION AND CLEARANCE IN MOTONEURON DISEASES

Riccardo Cristofani[1*], *Valeria Crippa*[1,2*], *Paola Rusmini*[1], *Maria Elena Cicardi*[1], *Marco Meroni*[1], *Nausicaa V. Licata*[1], *Gessica Sala*[3], *Elisa Giorgetti*[1], *Christopher Grunseich*[4], *Mariarita Galbiati*[1], *Margherita Piccolella*[1], *Elio Messi*[1], *Carlo Ferrarese*[3], *Serena Carra*[5§], *Angelo Poletti*[1,6§].

[1] Sezione di Biomedicina ed Endocrinologia, Dipartimento di Scienze Farmacologiche e Biomolecolari (DiSFeB), Centro di Eccellenza sulle Malattie Neurodegenerative, Università degli Studi di Milano, Milano, (Italy).

[2] Center for Research in Neurodegenerative Diseases (CRND), IRCCS "C. Mondino" Istituto Nazionale Neurologico, Pavia, (Italy).

[3] School of Medicine and Surgery, NeuroMI Milan Center for Neuroscience, University of Milano-Bicocca

[4] Neurogenetics Branch, National Institute of Neurological Disorders and Stroke, NIH, Bethesda, MD 20892, USA

[5] Dipartimento di Scienze Biomediche, Metaboliche e Neuroscienze, Università degli Studi di Modena e Reggio Emilia, Modena, Italy

[6] Centro InterUniversitario sulle Malattie Neurodegenerative, Università degli Studi di Firenze, Genova, Roma Tor Vergata and Milano, Italy

* The Authors equally contributed to this study.

§ Cocorresponding authors: Angelo Poletti, e-mail: <angelo.poletti@unimi.it> and Serena Carra, e-mail: <serena.carra@unimore.it>.

Dipartimento di Scienze Farmacologiche e Biomolecolari (DiSFeB), Università degli Studi di Milano - Via Balzaretti 9, 20133 Milano (Italy). ph. +39-02-50318215; fax: +39-02-50318204

RUNNING TITLE: TRANSPORT AND DEGRADATION OF MISFOLDED PROTEINS

KEYWORDS: Aggregation; amyotrophic lateral sclerosis; autophagy; BAG1; BAG3; HSPB8; misfolded protein; proteasome; protein quality control.

ABSTRACT

Motoneuron diseases, like spinal bulbar muscular atrophy (SBMA) and amyotrophic lateral sclerosis (ALS), are associated with proteins that because of gene mutation or peculiar structures, acquire aberrant (misfolded) conformations toxic to cells. To prevent misfolded protein toxicity, cells activate a protein quality control (PQC) system composed of chaperones and degradative pathways (proteasome and autophagy). Inefficient activation of the PQC system results in misfolded protein accumulation that ultimately leads to neuronal cell death, while efficient macroautophagy/autophagy-mediated degradation of aggregating proteins is beneficial. The latter relies on an active retrograde transport, mediated by dynein and specific chaperones, such as the HSPB8-BAG3-HSPA8 complex. Here, using cellular models expressing aggregate-prone proteins involved in SBMA and ALS, we demonstrate that inhibition of dynein-mediated retrograde transport, which impairs the targeting to autophagy of misfolded species, does not increase their aggregation. Rather, dynein inhibition correlates with a reduced accumulation and an increased clearance of mutant ARpolyQ, SOD1, truncated TARDBP/TDP-43 and expanded polyGP *C9ORF72* products. The enhanced misfolded proteins clearance is mediated by the proteasome, rather than by autophagy and correlates with the upregulation of the HSPA8 cochaperone BAG1. In line, overexpression of BAG1 increases the proteasome-mediated clearance of these misfolded proteins. Our data suggest that when the misfolded proteins cannot be efficiently transported towards the perinuclear region of the cells, where they are either degraded by autophagy or stored into the aggresome, the cells activate a compensatory mechanism that relies on the induction of BAG1 to target the HSPA8-bound cargo to the proteasome in a dynein-independent manner.

INTRODUCTION

Motoneuron diseases (MNDs) are neurodegenerative diseases (NDs) in which cortical and spinal motoneurons are primarily affected, although also other cell types (e.g., glial or muscle cells) contribute to onset and/or progression of disease.[1-11] Some MNDs forms are associated with the presence of toxic proteins with aberrant conformations (misfolded proteins).[12-15] Typical examples of MNDs associated with misfolded proteins toxicity are spinal and bulbar muscular atrophy (SBMA) and amyotrophic lateral sclerosis (ALS). SBMA is due to an expansion of the CAG repeat in exon 1 of the androgen receptor (*AR*) gene translated into an abnormally long polyQ tract in the AR (androgen receptor) protein (ARpolyQ).[16] Interestingly, elongated polyQ exerts neurotoxicity only after ARpolyQ activation by its natural ligand testosterone (T),[17] which implies chaperones release and protein conformational changes for nuclear translocation.[18] Protein misfolding is also relevant in ALS either in sporadic (sALS) or familial (fALS) forms, which are clinically indistinguishable. While fALSs represent only 10% of total ALSs, several fALS-responsible mutant proteins (e.g., SOD1 [superoxide dismutase 1, soluble], TARDBP/TDP-43 [TAR DNA binding protein], FUS, OPTN [optineurin], UBQLN [ubiquilin], etc.) have been found to aberrantly behave as wild-type (WT) forms also in most sALS,[19] suggesting that common pathogenic mechanisms contribute to both fALS and sALS.

To prevent misfolded protein toxicity, cells respond by enhancing the functions of the protein quality control (PQC) system. The PQC system comprises chaperone proteins (e.g., the heat shock proteins, HSPs) and degradative systems (e.g., the ubiquitin proteasome system, UPS; the different autophagic pathways, etc.). When poorly removed by the PQC system, misfolded proteins accumulate in cells forming different types of inclusions. Large cytoplasmic inclusions are generally thought to be protective, at least in their initial stages of formation,[18,20-23] Inclusions also localize into the nucleus or even in neurites exerting toxicity by altering several pathways regulating neuronal functions.[24,25] Inclusion formation proceeds through several steps. The process typically begins with the dynein and dynactin mediated transport of misfolded proteins escaping

proteasomal degradation to the microtubule-organizing center (MTOC), where they form aggresomes.[26] Aggresomes could be removed by autophagy, but, when this system fails, aggresomes are gradually converted into insoluble inclusions.

Several multiprotein complexes assist the misfolded proteins transport to the MTOC. One example is a complex involving the HSPB8 (heat shock protein 8) chaperone, a small HSP family member. HSPB8 promotes autophagic removal of misfolded proteins, including ARpolyQ, HTT (huntingtin)-polyQ, ATXN3 (ataxin 3)-polyQ, mutant SOD1, full-length TARDBP (FL-TARDBP) and its ALS-associated fragments, in different ND models.[27-33] HSPB8 acts together with BAG3 (BCL2-associated athanogene 3), a cochaperone of HSPA8/HSC70 (heat shock protein 8) and HSPA1A.[28,29,34-37] All these proteins are induced when the proteasome is inhibited[27-29] to route misfolded proteins to autophagy.[36,38] The ubiquitin ligase STUB1/CHIP (STIP1 homology and U-box containing protein 1) assists this complex by ubiquitinating clients[28,29,39] for their SQSTM1/p62 (sequestosome 1)-mediated targeting to phagophores, the precursors to autophagosomes.[40] BAG3 is a scaffold protein that plays a central role in autophagy.[41-45] With its proline-rich (PXXP) repeat motif it specifically bridges misfolded proteins to the dynein complex via the YWHA/14-3-3 protein, to allow their delivery to the MTOC for their autophagic degradation.[28,29,39,42] Several misfolded proteins found in aggresomes are not ubiquitinated,[46] and BAG3 activity can also be independent from their ubiquitination status.[42] Alternatively, aggresome formation is controlled by HDAC6 (histone deacetylase 6), which requires substrate ubiquitination; also HDAC6 interacts with dynein (through DCTN1/p150^{Glued} [dynactin 1]), but only after ubiquitination of substrates escaping UPS degradation,[47-51] and transports misfolded protein to MTOC.[47,49,52-54] Both BAG3-mediated and HDAC6-mediated clients routing to aggresomes require dynein.[26]

Notably, mutations in *DYNC1H1*, the gene coding for dynein (dynein cytoplasmic 1 heavy chain 1, the essential subunit of the cytoplasmic dynein complex) are linked to different neuronal diseases[55-62] involving autophagy alterations. Therefore, dynein impairment may have a role in neurodegeneration. Surprisingly, dynein activity deficiency correlates to improvement of motor

function and prolonged survival of the transgenic SOD1^{G93A} fALS mice [63-65] suggesting that the involvement of dynein in disease progression may be more compex than expected.

In this study, we analyzed the role of dynein on the clearance of misfolded ARpolyQ and of different proteins involved in ALS (human mutant SOD1, TARDBP, RAN translated polyGP from C9ORF72). We found that depletion or chemical inhibition of dynein decreased the aggregation of misfolded proteins and enhanced their proteasomal degradation. Dynein inhibition was paralleled by an upregulation of *BAG1* (BCL2-associated athanogene 1) expression, which targets the HSPA8 and HSPA1A-bound clients to the UPS.[38,66,67] Indeed, BAG1 overexpression enhanced misfolded protein degradation via the proteasome pathway even when dynein was inhibited. If BAG3 dynein-mediated transport of misfolded species to autophagy fails, an alternative pathway, which relies on BAG1 and the UPS, is activated to efficiently assist misfolded protein clearance. We postulate that the alteration of the rerouting system from autophagy to proteasome (and possibly *vice versa*) when one of the 2 degradative pathways is overwhelmed or impaired, rather than the alteration of the degradative pathway *per se* might be responsible for the accumulation of aggregate-prone proteins in MNDs.

RESULTS

HSPB8 promotes the clearance of misfolded ARpolyQ

We initially validated the prodegradative effect of HSPB8 on aggregated forms of ARpolyQ generated by T treatment. Fig. 1A shows that mutant ARpolyQ resides in the cytoplasm in basal conditions and translocates to the nucleus after T treatment. In approximately one third of total transfected cells[20,68] (see also Fig. 4F) nuclear translocation was incomplete and the misfolded ARpolyQ fraction aggregated as inclusions visible by immunofluorescence analysis (IF; Fig. 1A), and quantifiable in Filter Retardation Assay (FRA; Fig. 1B; compare lane 1 and lane 2, without or with T, respectively) in agreement with previous reports.[31,32,69] In basal conditions (T-untreated cells) ARpolyQ aggregation propensity is barely detectable and comparable to that of wild-type (WT) AR (see below and FRA in Fig. S1). The levels of insoluble WT AR (AR.Q23 in the absence or presence of T) and of T-untreated ARpolyQ (AR.Q46) were much lower than that found for T-activated ARpolyQ (Fig. S1, almost 2-fold increase over its control, untreated AR.Q46). We have already shown that the misfolded ARpolyQ accumulates upon T treatment, decreasing autophagy and leaving unaffected the proteasome,[31,32,69] and have found that the chaperone HSPB8 favors its degradation by autophagy. In line, here we show that both the T-induced cytoplasmic inclusions (Fig. 1A) and the insoluble ARpolyQ fraction (Fig. 1B, upper inset and quantification in bar graphs) disappear when HSPB8 is overexpressed, and the effect was present, at a lower intensity, on the total soluble ARpolyQ protein identified by western blot (WB; Fig. 1B lower inset, quantification in Fig. S2). No major effects are exterted by HSPB8 on WT AR.[32] Since HSPB8 requires BAG3 [30,34,70], for SQSTM1 cargo insertion into phagophores at the MTOC,[28,29,39] and BAG3 utilizes the dynein (and the YWHA/14-3-3 protein which cosegregates with ALS-protein aggregates[71-74])-mediated transport of the complex, we analyzed the role of dynein in HSPB8-mediated autophagic clearance of aggregates.

We designed a specific siRNA recognizing *Dync1h1* (*Dync1h1* siRNA) that abolished dynein production in NSC34 cells (Fig. 1C and Fig. 1D), and then we evaluated its effects on GFP-tagged ARpolyQ (GFP-AR.Q39) stably expressed in NSC34 cells in an inducible manner under the TetON promoter. Unexpectedly, after dynein downregulation, we found a significant reduction of the total amount of T-induced misfolded ARpolyQ insoluble species retained by the cellulose acetate membrane in FRA (Fig. 1E). In addition, a significant decrease of the total levels of ARs in WB was observed in dynein donwregulated samples, both in the case of unactivated ARpolyQ (normally processed by the proteasome) and of T-treated ARpolyQ (see WB quantification in Fig. S2).

Effects of dynein impairment on autophagy in basal conditions or after autophagy activation.

We next investigated whether dynein depletion correlated with a compensatory activation of autophagy. We initially evaluted the effects of dynein impairment in basal autophagy conditions in NSC34 cells. We measured the intracellular distribution and levels of the 2 autophagy markers SQSTM1 and MAP1LC3/LC3 (microtubule-associated protein 1 light chain 3). To our surprise, we found that in basal conditions, dynein downregulation does not alter the overall properties of these markers (Fig. 2A), suggesting that its impact on cargo delivery does not results in a compensatory activation of autophagy. However, since dynein may also regulate the fusion between the autophagosomes and lysosomes, we then further investigated the involvement of dynein on LC3 dynamics. To this purpose, we pharmacologically blocked the basal autophagic flux with NH_4Cl, and we found that the levels of the lipidated LC3-II form were similarly significantly increased by this treatment in all conditions tested (see quantification of LC3-II to TUBA and LC3-II to LC3-I ratio in Fig. 2B and Fig. S2, respectively). The relatively low LC3-II accumulation in the presence of NH_4Cl and almost constant levels of LC3-I (compare basal vs activated autophagy in Fig. 3D) are supportive of low levels of basal autophagic activity in these cells. Overall, these results support

preservation of basal autophagic flux even upon dynein knockdown and suggest that dynein has only a minor effect on the basal autophagic flux.

However, it is possible that, whereas *Dync1h1* siRNA is very efficient in each single cell, some cells may resist to transfection and dynein downregulation may not involve the whole cell population. Moreover, ATP-independent activities of dynein have been described,[75] with possible impact on different intracellular pathways. This promped us to adopt a second approach to block dynein-mediated transport. Therefore, we chemically and selectively blocked the ATP-dependent activity of dynein (specifically required for cargo delivery) with erythro-9-[3-2-(hydrosynonyl)] adenine (EHNA).[76,77] EHNA binds specifically to the ATP binding site of dynein inhibiting the ATPase and motor activities, selectively impairing the microtubule-based transport toward the MTOC. We initially compared the effects of EHNA with that of dynein-silencing in our NSC34 cells, by analyzing LC3-II levels in the presence or absence of NH_4Cl to block its lysosomal degradation (Fig. 2C and Fig. S2).

We found that the effects of dynein downregulation and of EHNA on the LC3 turnover and LC3-II to LC3-I ratio overlap in both conditions, supporting the view that dynein impairment has no effect on LC3 turnover in condition of basal autophagy (Fig. 2C and Fig S3). At present, we are unable to explain why and how autophagosomes assemble when autophagy is running at basal levels, and the relevance of dynein in this context. One possibility is that, even after siRNA or EHNA treatment, cells maintain a residual dynein activity, which may be sufficient to substain the autophagosome formation at low levels, or other alternative dynein-independent pathways of cargo delivery may exist. It is also possible that in condition of basal autophagy, the fusion between autophagosomes and lysosomes (which is required to degrade LC3-II into the autolysosomes) is only partially substained by dynein; the role of dynein may become more relevant when the flux is activated in response to specific stimuli. However, since misfolded proteins likely activate autophagy (and may also block autophagy),[32] we analyzed the effects of dynein impairment when autophagy flux was pharmacologically induced. To this purpose, we compared the alteration

induced by EHNA on autophagy in basal conditions or induced with trehalose (an MTOR-independent autophagy activator[31,32,78-80]). First, EHNA alone had no effect on *SQSTM1* or on *LC3* mRNA expression levels (Fig. 3A and 3B, respectively). Trehalose induced the expression of *SQSTM1* and *LC3* mRNAs; but, dynein inhibition with EHNA counteracted the effects of trehalose on the expression of the 2 autophagy markers (Fig. 3A and 3B). This suggests that cells respond to dynein inhibition with a downregulation of autophagy activation (and/or possibly by activating alternative pathways? see later). The data were confirmed also with both IF (Fig. 3C) and WB (Fig. 3D and quantification in Fig. S3) analyses. Trehalose-treated cells were highly immunoreactive (Fig. 3C, upper panels); to appreciate the effets of EHNA treatment (Fig. 3C, lower panels) images at a lower gain were captured (low sensitivity: L.S.). Indeed, trehalose increased endogenous SQSTM1 and LC3 protein levels (IF quantification per cells reported in bar graph of Fig. 3C, upper panels, and WB analysis in Fig. 3D, with relative quantification in the bar graphs and in Fig. S3) and induced the classical distribution expected for the 2 markers when autophagy is activated (i.e., LC3-II punctated distribution) (Fig. 3C). In basal conditions, EHNA does not modify the endogenous LC3 levels (Fig. 3C, see also Fig. 2C) or its conversion to LC3-II (Fig. 3C and 3D, and quantification in the lower bar graph and Fig. S3), while it significantly increased of almost 2-fold SQSTM1 immunoreactive levels in IF (Fig. 3C, left panels), and 1.7 fold in WB (Fig. 3D and S4). A difference has been found between the effects of dynein inhibition with ENHA and dynein downregulation with *Dync1h1* siRNA on SQSTM1 immunoreactivity quantify using confocal microscopy (compare Fig. 2A with Fig. 3C). However, as a small molecule, EHNA affects the entire pool of cells, while the siRNA only targets a fraction of them. Therefore, although both experimental approaches affect autophagy, differences can be observed in the 2 conditions. It is also possible that these differences are associated with the ATP-independent activities of dynein (see above and ref. 75).

During trehalose-stimulated autophagy, we found that EHNA reduced the overall levels of the endogenous SQSTM1 and LC3 proteins (IF in Fig. 3C), in agreement with the observed

transcriptional downregulation (Fig. 3A and Fig. 3B). Moreover, analysis of LC3-II degradation by addition of NH_4Cl, in cells with trehalose-stimulated autophagy (Fig. 3D and quantification in the lower bar graph and in Fig. S3), revealed that EHNA abolished the increase in LC3-II turnover induced by trehalose. These data suggest that dynein inhibition counteracts the formation of trehalose-induced LC3-II-positive autophagosomes, possibly by preventing their formation. Therefore, dynein inhibition with EHNA does not affect autophagy in basal conditions, but prevents the trehalose-stimulated formation of autophagosomes and this may in turn stimulate the activation of alternative pathways of degradation.

Dynein blockage reduces the ARpolyQ aggregation in an autophagy-independent manner

To test the role of dynein on ARpolyQ clearance we utilized different and complementary cell models of SBMA, based on neuronal cells stably expressing in an inducible manner or transiently expressing WT or mutant ARpolyQ. Based on data from literature of different laboratories, including ours,[20,25,31,32,69,81-87] as control for ARpolyQ we utilized either the WT AR (with unexpanded polyQ) or the unactivated (unbound) ARpolyQ (which is not pathogenic). When the experimental design was particularly complex, we compared the "neurotoxic" ligand activated ARpolyQ, with the "not neurotoxic" unactivated (nonpathogenic) ARpolyQ.[18,20,25,32,69,86-88]

We initially used rat pheochromocytoma PC12 cells stably expressing AR.Qn (n=112, and WT n=10, developed and kindly provided to us by Dr. Diane Merry, Thomas Jefferson University, Philadelphia, PA, USA[89]) with a very long polyQ tract highly prone to aggregate into the nucleus.[31,90] Using these models, in FRA (Fig. 4A), we found that T-induced misfolded AR.Q112 insoluble species formation, while EHNA reduced this accumulation (Fig. 4A). EHNA had no effects on T-untreated AR.Q112 or on WT AR (AR.Q10), which do not form insoluble inclusions (Fig. 4A). We then used mouse motoneuronal NSC34 cells stably expressing GFP-AR.Qn (n=39 and control n=0), where the mutant polyQ has a size that causes SBMA, but with late onset and low progression rate, and it is in the very low range of expansions identified in patients.[91-93] AR.Q39

does not form intracellular inclusions visible in IF (not shown), but it forms low amount of insoluble species detectable in FRA (Fig. 4C). As expected, control AR.Q0 does not form insoluble species, even after T treatment (Fig. 4B). Because of its shorter polyQ size, the AR.Q39 is likely to be less prone to misfolding than Q112. It is conceivable that AR.Q39 may have a milder impact than AR.Q112 on the degradative system (compare Fig. 4A and Fig. 4C); but, after its T activation, AR.Q39 is still mostly processed by autophagy (see also later in Fig. 5A, 3-MA-treated samples). Also in this case, EHNA significantly reduced the formation of T-induced misfolded AR.Q39 insoluble species to levels similar of that found in untreated AR.Q39 (Fig. 4C). No effects were seen on AR.Q0 (Fig. 4B). Interestingly, EHNA was also active on preformed inclusions (EHNA added 24 h after T treatment and maintained for other 24 h, Fig. S4), suggesting that these insoluble species are still dynamic at this stage.

Next, we enhanced the stressful conditions for motoneuronal cells by overexpressing proteins with transient transfection experiments, and used a polyQ tract of an intermediate size (Q46, which falls in the middle range of the pathological polyQ size described in SBMA patients[91-93]). The aim was to verify whether, by producing a large amount of misfolded ARpolyQ insoluble species, the effect of dynein-mediated transport blockage was still present. As shown in Fig. 4D, overexpression of AR.Q46 correlated with an accumulation of a large fraction of T-induced misfolded ARpolyQ-insoluble species. No accumulation was observed in untreated AR.Q46 (Fig. 4D; WB quantification in Fig. S3). The induction of ARpolyQ-insoluble species was similar (6-fold over control, Fig. 4A and Fig. 4D) in transiently transfected AR.Q46 (which aggregates in the cytoplasm[20,25,31,32,69,86,87] and Fig. 4E) and in stably transfected AR.Q112 (which aggregates in the nucleus[24,89,90]). Even with the overexpressing conditions, dynein inhibition with EHNA reduced the accumulation of T-induced misfolded ARpolyQ-insoluble species to levels comparable to those found in untreated ARpolyQ (Fig. 4D). Dynein inhibition with EHNA partially affected also the overall levels of the various AR.Qn utilized in these experiments (see WBs in 4A, 4C and 4D and quantified in S4). In parallel, with the reduced aggregated forms of the various AR.Qn, the decrease

(even if relatively small) of the overall T-treated ARpolyQ levels in WB, which comprises all SDS-soluble species (therefore, including the cytoplasmic ARpolyQ aggregates evaluated in IF), could be indicative of an increased clearance of the entire pool of the misfolded ARpolyQ fraction prior to its aggregation (see below). Another possibility is that by preventing ARpolyQ concentration and aggregation, chaperones might have a larger time-window to properly fold the mutant protein. This increased efficiency of chaperone activity might enhance the fraction of ARpolyQ detected in WB. Unfortunately, the relative contribution between clearance and correct folding of the mutant ARpolyQ allowed by dynein blockage is unpredictable and modifications of this balance explain why we observed some fluctuaction of the total levels of ARpolyQ in WB after EHNA treatment.

Next, using IF microscopy we examined the effects of dynein inhibition on the formation of intracellular inclusions of mutant AR.Q46 in NSC34 cells (Fig. 4E). In line with our previous observations, the presence of ARpolyQ cytoplasmic aggregates (present only in about 30% of total transfected cells, Fig. 4F) correlated with a decreased nuclear bioavailability of the AR protein (Fig. 4E, see second panel row).[20] In cells treated with EHNA, only few cells still contain aggregates, and in general, AR is free to migrate into the nucleus (Fig. 4E, see sixth and seventh panel rows) at levels comparable to that observed in EHNA-untreated T-treated cells with no cytoplasmic aggregates, in which ARpolyQ normally translocated into the nucleus (Fig. 4E, see third and fourth panel rows). Thereby, EHNA treatment counteracted the formation of cytoplasmic ARpolyQ inclusions induced by T (Fig. 4E), and this resulted in a higher localization of diffuse AR in the nucleus (Fig. 4E, compare different exposure times utilized). Quantification data, performed using GFP-tagged ARpolyQ, showed that EHNA treatment almost completely counteracted the formation of inclusion in NSC34 cells after T treatment, since the total number of inclusions found after dynein inhibition was similar to that found in control (T-untreated) cells (Fig 4E, F).

The WB in Fig. 4D, which represents the average of cells with or without aggregates, shows that the overall levels of soluble AR remains similar in the 2 conditions, apart from the fraction that is insoluble (as observed in FRA of Fig. 4D), which is indeed counteracted by EHNA.

Based on the observation reported above, we performed fractionation experiments using buffers characterized by increasing detergent power to analyse which particular insoluble fraction of ARpolyQ was mainly affected by EHNA treatment. The WB analysis on the solubilized pellets (see detailed scheme in Fig. S5), obtained after fractionation, revealed that cotreatment with EHNA and T increased the total levels of detergent-soluble AR.Q46, as compared to single treatment with T (Fig. 4G). This effect is possibly due to a shift between a phosphate-buffered saline (PBS)-Triton-insoluble fraction (likely associated with accumulating ARpolyQ in IF and FRA, and evaluated in the SDS-soluble fraction, (third inset)) to the PBS-Triton-soluble fraction of ARpolyQ (Fig. 4G [upper 2 insets]). Indeed, dynein inhibition increased the overall ARpolyQ content in NSC34 cell lysates (particularly in the PBS soluble fraction), and it also led to the complete removal of the ARpolyQ species present in the SDS-formic acid (FA) fractions (Fig. 4G). Some variability was found in the SDS/FA fractions obtained from T-treated NSC34 and AR.Q46 cells not exposed to EHNA. This is likely due to biological variations in the transition from a dynamic SDS-soluble (likely aggresomes, Fig. 4G, third inset) to a stable SDS-insoluble (likely inclusions, Fig. 4G, fourth inset) status of the ARpolyQ aggregating materials, in cells. This transition may occur in very few samples, since in our experimental condition the amount of SDS-insoluble species is negligible. Notably, since EHNA should prevent ARpolyQ concentration and thus reduce aggregation of misfolded species, it also prevents the accumulation of all the species detected after fractionation. Collectively, these data suggest that EHNA prevents misfolded ARpolyQ accumulation into insoluble species, possibly by reducing their concentration, a process favoring protein-protein interaction and aggregation.

Dynein inhibition reroutes ARpolyQ misfolded species from autophagy to proteasomal degradation.

Autophagy is the main degradative pathway for the disposal of aggregates, which can inhibit proteasome activities by clogging the proteasome. Since dynein modulation does not impair basal

autophagy, but maintains ARpolyQ in a soluble (likely monomeric) state compatible with proteasomal clearance, we investigated whether autophagy or proteasome inhibition affect the antiaggregating activity of EHNA. Fig. 5A shows that in AR.Q39 cells, when dynein is functional, both the inhibition of autophagy, with the inhibitor 3-methyladenine (3MA), or of the proteasome, with the inhibitor MG132, increased the levels of T-induced misfolded ARpolyQ insoluble species retained on the membrane by FRA. These species are considerably more abundant after 3MA than MG132 treatment, supporting that autophagy is the main degradative pathway activated by the cells to clear mutant ARpolyQ. Notably, in the case of the stably expressed AR.Q39, we found that this misfolded protein is characterized by a low tendency to aggregate (than with overexpressed AR.Q46 or stably expressed AR.Q112), possibly with low impact on autophagy flux. Indeed, after pharmacological autophagy blockage, T-induced misfolded AR.Q39 insoluble species accumulated at levels similar to those found in stably expressed AR.Q112 (compare with Fig. 4A; WB quantification in Fig. S3) or in transiently expressed AR.Q46 (compare with Fig. 4D; WB quantification in Fig. S3) after T treatment (about 6-fold over the corresponding untreated ARpolyQ). Therefore, the polyQ size may influence both the rate of misfolded AR autophagic clearance and the intensity of autophagy impairment associated with the presence of insoluble species.

Conversely, in NSC34-expressing AR.Q39 cells cotreated with T and EHNA, we found that inhibition of autophagy with 3MA had a lower impact on the accumulation of misfolded ARpolyQ insoluble species (Fig. 5A, compare lane 4 and lane 10; WB quantification in Fig. S6), suggesting that other degradative pathways, including the proteasome, may become more relevant to ensure ARpolyQ disposal. Indeed, when the proteasome was inhibited by MG132, the effect of EHNA was reduced (Fig. 5A), suggesting that proteasome, but not autophagy, is required to clear misfolded ARpolyQ insoluble species when their transport and concentration to MTOC is inhibited. Our hypothesis is that, in basal conditions, the proteasome with its narrow barrel-shape cannot properly digest misfolded ARpolyQ insoluble aggregate-prone species and these are targeted for degradation

to autophagy in a dynein-dependent manner. Instead, the inhibition of misfolded protein transport might delay their aggregation, which requires protein-protein interaction, a step largely favored by the concentration of proteins achieved via dynein-mediated transport to specific intracellular sites (e.g., the MTOC or other sites were autophagosomes could be generated). The inhibition of misfolded protein concentration will maintain the ARpolyQ into soluble (likely) monomeric forms digestible by the proteasome.

To test this hypothesis, we used the proteasome reporter GFPu, which consists of the GFP protein tagged with a short degron (CL1) that routes the protein to the proteasome for degradation.[86,94,95] Inhibition of the proteasome activity will result in GFPu accumulation into the cells.[31,32,69,87] We have already shown, and confirmed here (Fig. 5B and quantification in Fig. S6), that the unactivated ARpolyQ, normally processed by the proteasome, may compete with GFPu for degradation, leading to a reduced GFPu clearance; instead, the formation of T-induced misfolded ARpolyQ insoluble species correlated with proteasome desaturation (and enhanced GFPu clearance). In addition, we found that dynein inhibition with EHNA improved the clearance of GFPu in all conditions tested, proving that misfolded protein transport blockage has no effect on proteasome activity (Fig. 5B). Moreover, EHNA treatment does not alter the proteasome chymotryptic activity (Fig. 5C), even in presence of control or T-treated ARpolyQ (Fig. 5D). We then verified whether dynein inhibition with EHNA perturbs the global-mediated transcriptional (or the translational) activity of NSC34 cells (please note that the expression of all WT and mutant genes utilized in this study are under the control of the CMV promoter). As control, we evaluated the CMV-mediated transcription of the classical *lac*Z reporter gene measuring the encoded protein levels by testing the enzymatic β-galactosidase activity. In NSC34 cells, we found that the β-galactosidase activity was not affected by treatment with EHNA (Fig. 5E) indicating that dynein inhibition does not impair trascriptional regulation of CMV regulated genes. In addition, we evaluated whether ENHA treatment has effects on cell survival by evaluating cell viability using the MTT assay. No differences in the levels of mitochondrial formazan formation were observed

between control and EHNA-treated NSC34 cells (Fig. 5F), suggesting that at this concentration EHNA has no toxic effects on immortalized motoneuronal cells. Together these results exclude that the reduced levels of misfolded ARpolyQ insoluble species observed after EHNA treatment are a consequence of reduced protein synthesis and/or increased cell death. Instead, combined with the higher rate of the proteasome-mediated degradation of the GFPu reporter, these results support the hypothesis that cells treated with EHNA promote the degradation of mutant ARpolyQ with a mechanism that is dynein- and autophagy-independent, and seems to be proteasome-dependent.

So far, our data indicate that inhibition of dynein-mediated delivery of misfolded ARpolyQ species prevents their accumulation and aggregation in motoneuronal cells. Dynein inhibition does not increase proteasomal activity, but rather it might facilitate misfolded ARpolyQ species recognition by the proteasome, a process that requires them to remain into the monomeric status. It is known that chaperones targeting misfolded proteins to autophagy for degradation (such as the HSPB8-BAG3 complex associated with HSPA8- and HSPA1A-bound substrates[27-29,38,96]) are generally upregulated when the proteasome is impaired. We asked whether EHNA tretament may activate an alternative chaperone response. We focused on BAG1, which, like BAG3, is a member of the BAG family of nucleotide exchange factors. In alternative to the HSPB8-BAG3 complex, BAG1 targets HSPA8- and HSPA1A-bound substrates to the proteasome for disposal.[38,66,67,97] Interestingly, after EHNA treatment, both *Hspb8* (Fig. 6A) and *Bag3* (Fig. 6B) mRNA levels remained unchanged in NSC34 cells, while *Bag1* expression increased to over 2.5-fold supporting our working hypothesis (Fig. 6C). We next tested the functional significance of BAG1 upregulation on misfolded ARpolyQ clearance upon inhibition of dynein-mediated transport. Overexpression of BAG1 significantly reduced the accumulation of ARpolyQ retained on the cellulose acetate membrane (FRA, Fig. 6D; WB quantification in Fig. S6). Since BAG1 targets HSPA8- and HSPA1A-bound clients to the proteasome for degradation, we also evaluated whether the BAG1 prodegradative function depends on a functional proteasome. In agreement with previous reports,[97] we found that proteasome inhibition prevented the BAG1 prodegradative activity on T-inducible

misfolded ARpolyQ insoluble species in NSC34 cells (Fig. 6E). Therefore BAG1, which is upregulated upon dynein inhibition with EHNA, enhances the proteasome-mediated degradation of ARpolyQ, limiting ARpolyQ aggregation linked to its "concentration" mediated by dynein, and protein "concentration" is required for selfassociation combined with insufficient autophagy for proper disposal. To further test this hypothesis, we downregulated endogenous *Bag1* expression with a specific siRNA in NSC34 cells (Fig. 6F). Depletion of *Bag1* in NSC34 cells expressing mutant ARpolyQ led to an increase in the levels of soluble and aggregated AR.Q46 species, both in absence and presence of T, supporting that BAG1 participates in ARpolyQ clearance. Depletion of *Bag1* also significantly decreased the antiaggregation function of EHNA, since aggregated AR.Q46 accumulated at higher levels as compared to control cells (Fig. 6G, compare lanes 3, 4 with lanes 7, 8; WB quantification in Fig. S6). Notably, in agreement with our previous reports demonstrating that "nontoxic" and soluble T-untreated AR.Q46 is mainly processed by the proteasome,[69,86,87] *Bag1* silencing increased the accumulation of unactivated AR.Q46.

Based on our findings we propose that, when the cells cannot transport misfolded ARpolyQ to the authophagosomes or aggresomes for its dynein-dependent autophagy-mediated degradation, they induce the expression of BAG1 to target these species to the proteasome for clearance.

Rerouting of misfolded ARpolyQ in SBMA patient-derived iPSCs differentiated to neuronal and motoneuronal cells.

To extend our observations to a more reliable model that better recapitulates the conditions present in human motoneurons of SBMA patients, we used a cell model alternative to NSC34 or PC12 cells, the motoneuronal cells obtained by differentiation of human induced pluripotent stem cells (iPSCs) to neuronal cells generated from SBMA patients. These cells have been cultured both in basal condition or exposed to T to induce ARpolyQ misfolding and toxicity. Differentiation of iPSCs was performed using the protocol described by Grunseich et al.[98] (who developed the SBMA iPSCs), which allows to produce "*bona fide*" neuronal cells (all positive for neuronal markers including

TUBB3 and the axonal specific marker SMI312; Fig. 7A) and enriched of a variable population of motoneuronal cells which ranges from 15 to 23% (positive for motor neuron and pancreas homeobox 1 (MNX1/HB9) marker, Fig. 7A and quantification in Fig. 7B) of the total neuronal population. No glial cells were observed using the differentiation protocol adopted here.[98] All iPSCs differentiated to neuronal cells from SBMA patients were also positive for AR expression, which translocated to nucleus upon T treatment (Fig. 7A). No major morphological variation was observed for neuronal and motoneuronal markers after T treatment (Fig. 7A and 7B).

Interestingly, after EHNA treatment, *HSPB8* mRNA levels remained unchanged in iPSCs differentiated to neuronal cells (both untreated or T-treated) (Fig. 7C); *BAG3* expression was mildly induced by T and to a lower extend by EHNA (Fig. 7D). EHNA treatment increased the expression of *BAG1* of almost 1.5-fold and 2.5-fold in untreated and T-treated iPSCs differentiated to neuronal cells, respectively (Fig. 7E), further supporting that *BAG1* upregulation represents a physiological stress response upon dynein inhibition. We next evaluated the impact of EHNA on the expression of key autophagy proteins in iPSCs differentiated to neuronal cells. After dynein inhibition (both in the absence and in the presence of T), the mRNA levels of *SQSTM1* and TFEB (transcription factor EB) were increased (Figs. 7F, 7H), while *LC3* levels remained unmodified after EHNA tretament (Fig. 7G). Notably, this upregulation of *TFEB* and *SQSTM1* could be a cell attempt to restore an altered autophagic flux or to improve the intracellular lysosomal activity when transport of cargo to the autophagosomes is blocked. Conversely, *BECN1* remained unchanged by dynein inhibition in iPSCs differentiated to neuronal cells (Fig. 7I). Combined these results strongly support that BAG1 is a crucial physiologically activated PQC player.

Effects of dynein inhibition on the clearance of other misfolded proteins associated with motoneuron diseases

We next wanted to investigate whether the effects of dynein inhibition with EHNA described above are specific for the mutant misfolded ARpolyQ or are also exerted on other mutant proteins

responsible for another motoneuron disease similar to SBMA, the ALS. We selected 2 proteins that have been associated with ALS: i) the SOD1 enzyme (mutated in about 20% of fALS),[99] and ii) a truncated form of TARDBP (TARDBP$^{\Delta C}$, found in some fALS cases). Both mutant SOD1^{G93A} and TARDBP$^{\Delta C}$ misfold and accumulate into cytoplasmic aggregates; as shown for ARpolyQ [31,32] their autophagic clearance can be enhanced by the HSPB8-BAG3 complex.[28,29,32,96] In 2 different models of ALS, SOD1^{G93A} transiently (Fig. 8A; WB quantification in Fig. S6) or inducible stably transfected (Fig. 8B) motoneuronal NSC34 cells, EHNA treatment resulted in a reduction of the total amount of misfolded mutant SOD1 insoluble species accumulating on cellulose acetate in FRA. Similar results were obtained in ALS models generated using the TARDBP$^{\Delta C}$ mutant (Fig. 8C; WB quantification in Fig. S7), demonstrating that dynein inhibition also affects the accumulation of the truncated fragment of TARDBP involved in ALS. As in the case of ARpolyQ, EHNA activity requires a functional proteasome activity, since its inhibition with MG132 prevented (even if not completely, see below) the clearance of mutant SOD1 (Fig. 8D; WB quantification in Fig. S7) and TARDBP$^{\Delta C}$ (Fig. 8E; WB quantification in Fig. S7), observed after dynein inhibition. Conversely, EHNA exerted its prodegradative effect on these 2 ALS-associated proteins when autophagy was inhibited by 3-MA treatment (Fig. 8D and 8E; WB quantification in Fig. S7).

Finally, we wanted to further extend these observations to other forms of proteinaceuos aggregates also involved in motoneuron diseases, but structurally totally distinct from the misfolded proteins studied above. We analyzed one out of 5 potentially neurotoxic dipeptides generated by RAN-translation from the *C9ORF72* transcript containing an expanded exanucleotide repeat (GGGGCC)n linked to several fALS (and some sALS) cases and in many cases of frontotemporal dementia.[100-106] To produce the peptide selected (the dipeptide [glycine-proline], polyGP) we used a synthetic DNA in order to avoid multiple dipeptide production and/or (GGGGCC)n-associated RNA toxicity.[107] The polyGP is not produced in basal physiological conditions and it is likely that the polyGP has no propensity to acquire a natural conformation. It is expected that its structure is likely to be unrelated to the aberrant conformation generated by the mutant misfolded proteins.

Despite this, also the polyGP is prone to aggregate, and accumulates in neurons into intracellular insoluble inclusions. The polyGP is cleared by the PQC system,[107] an aspect that we confirmed in immortalized motoneurons, where both proteasome or autophagy inhibition (with MG132 or 3MA, respectively) increased the accumulation of insoluble polyGP species evaluated with FRA (Fig. 9; WB quantification in Fig. S7). In line with our previous data, dynein inhibition led to a reduction of polyGP insoluble species even when autophagy is blocked with 3MA. In the case of polyGP, the antiaggregant effect of ENHA was not completely counteracted by the cotreatment with the proteasome inhibitor MG132, even if more than 50% of total insoluble polyGP species accumulated with proteasome blockage. PolyGP is characterized by a very high proteasomal turnover. Indeed, we found a 30-fold increase of insoluble species accumulating with MG132 treatment. Since MG132 only inhibits the chymotryptic proteasomal activity,[108,109] it is likely that the polyGP will be processed also using the postacidic or tryptic activities of the proteasome, which may explain the partial inhibitory effect obtained by treatment with MG132. Alternatively, as already postulated above, other degradative pathways (such as chaperone mediated autophagy [CMA]) could be involved in the polyGP clearance, as well as for ARpolyQ, mutant SOD1, TARDBP in which proteasome inhibition did not always correlate with a full blockage of EHNA effects.

DISCUSSION

Here, we analyzed how the inhibition of the dynein-mediated retrograde transport of misfolded proteins to MTOC affects their intracellular aggregation and clearance. Our approach was based on previous data showing that misfolded protein clearance is enhanced by their interaction with the complex HSPB8-BAG3,[28,29] a complex that, in conjunction with HSPA8 and HSPA1A, recruits STUB1 to allow misfolded substrate ubiquitination and SQSTM1 mediated insertion into autophagosomes at the MTOC.[39] BAG3 interacts with the YWHA/14-3-3 protein and dynein, which transports the complex (misfolded protein-HSPB8-BAG3-HSPA8-STUB1) to the MTOC.[73,74] Given this evidence, we were expecting that dynein inhibition correlated with an overall increased accumulation of insoluble and aggregated misfolded proteins inside the cells. Instead, in motoneuronal cells, we found that depletion or chemical inhibition of dynein decreased the aggregation of misfolded proteins maintaining them in a soluble state competent for proteasomal degradation. In fact, upon dynein inhibition, all misfolded proteins we analyzed were preferentially targeted to the proteasome for degradation, while autophagy inhibition had no or mild impact on their total levels and aggregation. Dynein inhibition did not impair basal autophagy, which appeared to be very limited in basal conditions in our cells. Conversely, dynein inhibition reduced activation of autophagy stimulated by trehalose, mostly through changes at the transcriptional level.

Misfolded proteins species altered autophagy, but dynein blockage reduced their disposal via autophagy. Under these conditions, the autophagy markers, *HSPB8* and *BAG3* were not induced, while *BAG1* was upregulated. BAG1 is a HSPA8 cochaperone which both assists HSPA-mediated protein folding (by enhancing its activity as nucleotide exchange factor),[38,66,67] and targets HSPA8 client proteins to proteasomal degradation[66,97,110-113] (and under specific circumstances even to CMA[114]). Our results suggested that BAG1 represents a crucial player by routing misfolded proteins to proteasome when their transport to the MTOC is blocked. In line, overexpression of

BAG1 in cells with deficient or inhibited dynein allowed a more efficient proteasomal degradation of misfolded species that were accumulating in a monomeric, or small oligomeric and soluble forms, rather than as aggregates because of the inhibition of their concentration at the MTOC (a process that facilitates aggregation).

Conversely, because proteasome inhibition leads to upregulation of BAG3 and HSPB8, which reroute (poly)-ubiquitinated and misfolded clients towards autophagy for degradation,[28,29,38] here we propose that, in cells where dynein-mediated transport is inhibited, BAG1 upregulation and its mediated rerouting of misfolded substrates to the proteasome represent an alternative mechanism activated by cells to maintain protein homeostasis. Molecularly, this may be explained by the fact that BAG1 possesses an ubiquitin-like domain for targeting of the HSPA8-bound client to the proteasome, while BAG3 has no ubiquitin-like domains,[37,115-117] but its interaction with YWHA/14-3-3-dynein permits the transport of misfolded proteins to the MTOC for autophagy clearance.[70,73,74] Therefore, when misfolded proteins cannot be efficiently transported to autophagosomes, the cells upregulate an alternative chaperone system, that ensures enhanced proteasomal misfolded proteins clearance preventing their aggregation. In line, pharmacological autophagy blockage did not alter the effect of dynein inhibition on misfolded protein clearance. The prevention of misfolded protein concentration also might reduce protein-protein interaction, which is essential for aggregation, favoring the maintenance of the monomeric status of the protein. This might allow a larger time window for proper protein folding, since BAG1 also acts as a nuclear exchange factor for HSPA, enhancing and optimizing its chaperone activity and this acts alternatively to protein rerouting to the proteasome. This may explain why we occasionally found variations in the total levels of soluble ARpolyQ (measured in WB), as compared to the levels of insoluble ARpolyQ (detected with FRA), after EHNA treatment. Even if both folding and degradation processes may coexist, our data suggest that the role of degradation prevails on the refolding. Here we propose that dynein inhibition requires 2 steps: 1) control of aggregation and 2) routing of soluble clients towards the proteasome (or to proper folding) in a BAG1-assisted manner. In fact, under these conditions,

insertion of aggregate-prone proteins into an aggresome is blocked [46,118] and the aggregate-prone substrates are maintained in a state that is competent for degradation by the proteasome.[119]

Notably, also preformed (but still dynamic) aggregates can be redissolved into soluble proteasomal digestible proteins, since EHNA was also effective when added 24 h after ARpolyQ inclusions induction with T. The rerouting system here described might also have impact on nuclear inclusions. Indeed, we showed that also using an ARpolyQ with a very long size (Q112), which is capable of generating nuclear aggregates, resembling those typically found in SBMA patients,[24,25] dynein blockage correlated with a reduced accumulation of insoluble species, possibly associated with enhanced proteasomal clearance taking place both in nuclear and cytoplasmic compartments.

Altogether, these data shed light on the importance of dynein-mediated transport in the intracellular routing of misfolded proteins to their preferred degradative system, and are in line with previous observations showing that the disruption of microtubules with nocodazole inhibits aggresome formation in cells expressing the exon 1 of mutant HTT (huntingtin) or ARpolyQ.[46,118,120] These studies also showed that prevention of aggregate formation correlates with an increased toxicity of the 2 misfolded proteins analyzed (HTT-polyQ and ARpolyQ), supporting the notion that aggresomes may have a protective activity in their earlier stages of formation.[20-22] In our study, a less invasive and more specific approach was used to block misfolded protein concentration at the MTOC, where aggresomes are formed.[121,122]

Therefore, it is likely an alteration of the fine equilibrium of protein routing that may affect the release or accumulation of neurotoxic species, rather than the impairment or overwhelming of a single degradative pathway. These pathways may also include CMA. Indeed, BAG1, by interacting with HSPA8, might also direct misfolded proteins to CMA for clearance,[114,119,123] Unfortunately, no selective inhibitors are available for CMA and we were unable to evaluate its contribution in the degradation of misfolded species after dynein impairment.

A second aspect that emerges from the data here presented is that the role of dynein in mediating the transport of autophagosomes to lysosomes to allow their fusion may be secondary to

the cargo delivery to the MTOC. In fact, we did not find major problems in misfolded protein clearance even if autolysosome formation was impaired in parallel to transport blockage. As stated above the activity of this pathway is made irrelevant by the BAG1-mediated routing of misfolded proteins to the proteasome (and eventually CMA), and the role of dynein in cargo transport to phagophores precedes that in autophagosome and lysosome fusion.

These data apparently contrast with the observations obtained in transgenic mice carrying missense point mutations in the cytoplasmic dynein heavy chain. Heterozygous mice are characterized by progressive motoneuron loss, but without accumulation of proteinaceous material in affected cells. Homozygous mice suffer motoneuronal degeneration with accumulation of Lewy-like inclusion bodies.[60] In addition, cytoplasmic dynein is activated by the ubiquitously expressed dynactin, and mutation in the DCTN1/p150^{Glued} subunit of dynactin, which prevents dynein activation, causes specific motoneuron loss, with the appearance of DCTN1/p150^{Glued} protein aggregates[124-126] (see also ref. 127 for an extensive review on dynein mutations in human and mice). However, different mice in which dynein and dynactin functions are altered (either because of dynein mutations (Legs at odd angles),[65,128] or because of neuron-specific expression of Bicaudal D2 N-terminus[129]) causing an ALS-like phenotype, have improved life span when crossed with transgenic SOD1^{G93A} mice.[65,128,129] The phenotype of these double transgenic mice is also ameliorated when compared to the single transgenic mice expressing the mutant SOD1 protein. Therefore, while dynein mutations *per se* are deleterious to motoneurons, it is possible that dynein may contribute to exacerbate the adverse effects exerted by mutant misfolded proteins on motoneurons. It is likely that this adverse effect of dynein is due to a routing of misfolded proteins at the MTOC (which escape proteasome-mediated degradation) that induces aggregation and possibly autophagic flux blockage.

While these data may not be readily translated into possible therapeutic approaches, they could help to better understand the molecular mechanisms at the basis of misfolded protein clearance and the way that motoneurons select specific pathways of degradation for a given protein.

MATERIALS AND METHODS

Chemicals

Erythro-9-(2-Hydroxy-3-nonyl) adenine hydrochloride (EHNA; Sigma-Aldrich, E114), Z-Leu-Leu-Leu-al (MG132; Sigma-Aldrich, C2211), trehalose (Sigma-Aldrich, T9531), 3-methyladenine (3MA; Selleckchem, S2767), ammonium chloride (Euroclone, EMR089500).

Plasmids and siRNA

The plasmids coding for AR.Q23, AR.Q46, GFP-AR.Q48 and pCI-HSPB8 are routinely used in our laboratory and they have been previously described.[20,30-32] The pcDNA/HA-BAG1 plasmid coding for the protein BAG1 was kindly provided by Prof. Harm H. Kampinga (University of Groningen, Groningen, The Netherlands).[67,130] The plasmid expressing the proteasome function reporter GFPu was kindly provided by Prof. Ron Kopito (Stanford University, Stanford, CA, USA).[94] The pCMV-β plasmid, encoding β-galactosidase (Clontech, 6177-1) was used to evaluate EHNA effect on total protein expression levels. The pcDNA3-wtSOD1 and pcDNA3-SOD1^{G93A} plasmids expressing human wtSOD1 or mutant SOD1^{G93A} were kindly provided by Dr. Caterina Bendotti (Mario Negri Institute, Milano, Italy).[131] pFLAG-FL TDP-43 (TARDBP), and pFLAG-TDP-43$^{\Delta C}$ (TARDBP$^{\Delta C}$) plasmids, expressing FLAG-tagged full-length human TARDBP and an N terminal truncated at residue 261 (lacking the C-terminal region), respectively, were kindly provided by Dr. Emanuele Buratti (International Centre for Genetic Engineering and Biotechnology, Trieste, Italy).[132,133] pCMV-Flag-polyGP-V5-His plasmid encoding the polyGP dipeptide was kindly provided by Prof. Daisuke Ito (Keio University School of Medicine, Tokio, Japan).[107] The pcDNA3 (Life Technologies, V790-20) plasmid was used to normalize for transfected plasmid DNA amount. The pEGFPN1 (Clontech, U55762) plasmid was used to evaluate transfection efficiency in experiments involving transient transfections. pcDNA5/TO-GFPAR.Q0 and pcDNA5/TO-GFPAR.Q39 plasmids were used to obtain stable and inducible SBMA cell models and were constructed by cloning the sequence coding for GFPAR.Q0 and GFPAR.Q39 into NheI and XbaI sites of

pcDNA5/TO (Life Technologies, V103320), previously modified with insertion of BamHI and NheI sites.

To silence endogenous *Dync1h1* and *Bag1* expression we used custom siRNA duplex: [5'-GGGUAAAGCUAGAGAGAAUUU-3' (sense)], [5'-AUUCUCUCUAGCUUUACCCUU-3' (antisense)] for *Dync1h1* and [5'-AAGAAGAGGUUGAGUUAAAUU-3' (sense)], [5'-UUUAACUCAACCUCUUCUUUU-3' (antisense)] for *Bag1* (Dharmacon, Thermo Scientific Life Sciences Research).

Cell cultures and transfection

The immortalized motoneuronal cell line NSC34[134,135] is routinely used in our laboratory and has been transfected with Lipofectamine (Life Technologies, 18324020)-TRF (transferrin; Sigma-Aldrich, T8158), as previously described,[20,25,136] using 0.6 μg of plasmid DNA, 4 μL of TRF solution and 2 μL of Lipofectamine (amount for 1 well of a 12-well multiwell plate). siRNA transfection was performed with Lipofectamine 2000 (Life Technologies, 11668019), using 40 pmol of target RNA and following the manufacturer's instructions.

Inducible stably transfected NSC34-GFPAR.Q(n) cell lines were obtained by transfecting pcDNA5/TO-GFPAR.Q(n) into TR4 NSC34 cell line stably transfected with pcDNA6/TR encoding for tetracycline repressor, kindly provided by Dr. Enrico Garattini (Mario Negri institute, Milan, Italy), and were routinely maintained as described previously.[137]

Rat adrenal pheochromocytoma (PC12) cells stably transfected with the plasmid encoding AR.Q10 and AR.Q112 express AR under the control of a Tet-On promoter, responsive to 1 μg/mL of doxycycline. PC12-AR.Q(n) cells have been produced and kindly provided by prof. Diane Merry (Thomas Jefferson University, Philadelphia, PA, USA) and were routinely maintained as described by Walcott et al., 2002.[89]

iPSCs were obtained in the lab of Dr. Kennet Fischbeck (by Dr. Christopher Grunseich) at NIH, Bethesda, MD, USA from fibroblasts of SBMA patients (SB6MP2 clone) and generated by

POU5F1/Oct4, KlF4, SOX2 and MYC/c-Myc transfection. iPSCs were cultured in Essential 8 medium (Life Technologies, A1517001) and differentiated into motoneurons as described previously.[98] Briefly, iPSCs were grown to 80% confluency, then digested with collagenase IV (Life Technologies, 17104019), scraped off of the dish, and replated into ultra-low attachment dishes (Corning, 3262) in KSR (Life Technologies, 10828028)-based medium, with 20 ng/ml FGF (ORF genetics, 01-A01110), 20 μM ROCK-I (Selleckchem, S1049), 10 μM SB431542 (Stemgent, 04-0010), 0.2 μM LDN193189 (Stemgent, 04-0074), to allow embryo bodies (EBs) formation. EBs were transitioned to a KSR-free medium at day 3. Retinoic acid (1 μM; Sigma-Aldrich, R2625) was added at day 5 to direct cell differentiation into the rostral spinal cord phenotype. Smoothened agonist (1 μM; Merck Millipore, 566660) and 0.5 μM purmorphamine (Caymanchem, 10009634) were added at day 7 to ventralize the differentiating population. The EBs were dissociated at day 14 and plated at 150,000 cells/well on 12-well multiwell plates for RNA extraction or at 50,000 cells/well on 24-well multiwell plates for immunofluorescence (IF). Plates were coated with poly-D-lysine (Sigma-Aldrich, P7405) and laminin (Life Technologies, 23017015). Differentiated-motoneurons were allowed to grow for an additional 10 days in neurobasal medium (Life Technologies, 21103049) with 25 μM glutamate (Sigma-Aldrich, 1446600), 0.4 μg/ml ascorbic acid, 10 ng/ml GDNF (PeproTech, 167450-10), 10 ng/ml CNTF (PeproTech, 167450-13), 1 μg/ml laminin, B-27 (Life Technologies, 17504044), N2 (Life Technologies, 17502048), nonessential amino acids (Euroclone, ECB3054D), and pen/strep/glutamine (Euroclone). Motoneuronal cells were treated with ethanol or 10 nM T and/or 100 μM EHNA for the last 48 h previous to analysis.

Stably transfected NSC34-wtSOD1 and NSC34-SOD1^{G93A} cell lines have been produced and kindly provided by Prof. Maria Teresa Carrı` (Università Roma Tor Vergata, Roma, Italy). These cell lines express MYC-tagged human wtSOD1 or SOD1^{G93A} and were routinely maintained as described by Ferri and colleagues.[138]

In the experiments involving steroid hormone treatments, the serum was replaced with charcoal-stripped serum, to eliminate endogenous steroids.[25,139,140] The effects of treatments (T,

EHNA, 3MA, MG132, etc.), for each mutant protein considered, were analyzed on 3 (4 for the RT-qPCR analysis) independently cultured, transfected and treated samples (considered as independent variables (n)).

mRNA expression analysis

NSC34 cells were plated at 180,000 cells/well (4 wells for each condition to be tested; n=4) in 6-well multiwell plates, allowed to growth for 24 h and then treated with 100 μM EHNA and/or with 100 mM trehalose, or with DMSO (used as negative control). Forty-eight h after treatments, cells were harvested and centrifuged 5 min at 100 x g at 4°C; the pellets were resuspended in 300 μL of TRI Reagent (Sigma-Aldrich, T9424) and total RNA isolated according to manufacturer's instructions. RNA quantification was carried out by absorbance at 260 nm. Total RNA (1 μg) was treated with DNAse I (Sigma-Aldrich, AMPD1), and reverse transcribed into cDNA using the High-Capacity cDNA Archive Kit (Life Technologies, 4368813) according to the manufacturer's protocol. All primers for real-time PCR were designed using the program Primer 3.

The primers were synthesized by MWG Biotech (Ebersberg, Germany) with the following sequence: *Map1LC3-B*: 5′-CGT CCT GGA CAA GAC CA-3′ (forward), 5′-CCA TTC ACC AGG AGG AA-3′ (reverse); *Sqstm1*: 5′ -AGG GAA CAC AGC AAG CT-3′ (forward), 5′ -GCC AAA GTG TCC ATG TTT CA-3′ (reverse); *Rplp0*: 5'-GGT GCC ACA CTC CAT CAT CA-3' (forward), 5′ -AGG CCT TGA CCT TTT CAG TAA GT-3′ (reverse); *Hspb8*: 5'-ATA CGT GGA AGT TTC AGG CA-3' (forward), 5′ -TCT CCA AAG GGT GAG TAC GG-3′ (reverse); *Bag3*: 5'-ATG GAC CTG AGC GAT CTC A-3' (forward), 5′ -CAC GGG GAT GGG GAT GTA-3′ (reverse); *Bag1*: 5'-GAA ACA CCG TTG TCA GCA CT-3' (forward), 5′ -GCT CCA CTG TGT CAC ACT C-3′ (reverse); *HSPB8*: 5'- AGA GGA GTT GAT GGT GAA GAC C-3' (forward), 5′-CTG CAG GAA GCT GGA TTT TC-3′ (reverse); *BAG1*: 5'-TTT AGA GCA GCC CGA GTG AT-3' (forward), 5′-GAC AGC AGA CAG CCA ACA AA-3′ (reverse); *BAG3*: 5'- GGG TGG AGG CAA AAC ACT

AA-3' (forward), 5′-AGA CAG TGC ACA ACC ACA GC-3′ (reverse); *SQSTM1* 5'- CCA GAG AGT TCC AGC ACA GA-3'(forward), 5'- CCG ACT CCA TCT GTT CCT CA-3'(reverse); *MAP1LC3B* 5'- CAG CAT CCA ACC AAA ATC CC-3'(forward), 5'- GTT GAC ATG GTC AGG TAC AAG-3'(reverse); *TFEB* 5'- CAA GGC CAA TGA CCT GGA C-3'(forward), 5'- AGC TCC CTG GAC TTT TGC AG-3'(reverse); *BECN1* 5'-ATG CAG GTG AGC TTC GTG TG-3'(forward), 5'-CTG GGC TGT GGT AAG TAA TGG A-3'(reverse); *RPLP0*: 5'-GTG GGA GCA GAC AAT GTG GG-3' (forward), 5′-TGC GCA TCA TGG TGT TCT TG-3′ (reverse).

The evaluated efficiency of each set of primers was close to 100% for both target and reference gene. Real-time PCR was performed using the CFX 96 Real-Time System (Bio-Rad, Hercules, CA, USA) in a 10-µL total volume, using the iTaq SYBR Green Supermix (Bio-Rad, 1725124), and with 500 nM primers. PCR cycling conditions were as follows: 94°C for 10 min, 40 cycles at 94°C for 15 sec and 60°C for 1 min. Melting curve analysis was performed at the end of each PCR assay as a control for specificity. Data were expressed as C_t values and used for the relative quantification of targets with the $\Delta\Delta C_t$ calculation.[141,142] To exclude potential bias due to averaging, data have been transformed through the equation $2^{-\Delta\Delta C_t}$ to give N-fold changes in gene expression, all statistics were performed with ΔC_t values. Each experiment was carried out with 4 independent samples (n=4).

Western blot (WB) analysis and filter retardation assay (FRA)

NSC34 or PC12 cells were plated in 12-well multiwell plates at 80,000 cell/well (3 wells for each condition to be tested; n=3). 24 h after plating, cells were transfected as previously described or induced with 1 µg/mL doxycycline, and AR activation was induced by 10 nM T treatment for 48 h. Inhibition of dynein ATPase activity was performed by 100 µM EHNA for 48 h. In experiments involving autophagy blockage or induction, 10 mM 3MA for the last 48 h, 20 mM NH_4Cl for the last 1.5 h or 100 mM trehalose for the last 48 h were added to the cells. Proteasome inhibition was

performed by 10 μM MG132 treatment for the last 16 h (overnight treatment). Seventy-two h after plating, cells were harvested and centrifuged 5 min at 100 x g at 4°C; the cell pellets were resuspended in PBS (Sigma-Aldrich, P4417) added of the protease inhibitor cocktail (Sigma-Aldrich, P8340) and homogenized using slight sonication to lyse cells and nuclei as previously described.[86,139] Total proteins were determined with the bicinchoninic acid method (BCA assay; Euroclone, EMP014500).

WB was performed on 7.5% (to detect AR protein), 12% (to detect SOD1 and TARDBP proteins) or 15% (to detect LC3 and SQSTM1/p62 proteins) SDS-polyacrylamide gel electrophoresis loading 15 μg of total proteins. Samples were then electrotransferred to nitrocellulose (Bio-Rad, 1620115) or PVDF (polyscreen transfer membrane; Amersham, 10600023) using a semidry transfer apparatus (Trans-Blot^{w} Turbo^{TM} Transfer System; Bio-Rad). The membranes were treated with a blocking solution containing 5% nonfat dried milk powder (Euroclone, EMR180500) in Tris-buffered saline with Tween 20 (0.01%; Sigma, P1379) (TBS-T; Tris base 20 mM, NaCl 140 mM, pH 7.6) for 1 h and then incubated with one of the following primary antibodies: (a) rabbit polyclonal AR-H280 (dilution 1:3,000) to detect wtAR and ARpolyQ (Santa Cruz Biotchnology, sc-13062); (b) rabbit polyclonal anti-LC3A/B (dilution 1:4,000; Sigma-Aldrich, L8918); (c) rabbit polyclonal anti-SQSTM1 (dilution 1:4,000; Abcam, ab91526); (d) rabbit polyclonal anti-dynein heavy chain (dilution 1:1,000; Santa Cruz Biotchnology, sc-9115); (e) rabbit polyclonal anti-GFP HRP conjugated (dilution 1:15,000; Vector Laboratories, MB-0712); (f) rabbit polyclonal anti-HA (dilution 1:1,000; Santa Cruz Biotchnology, sc-7392) to detect overexpressed BAG1; (g) rabbit polyclonal anti-BAG1 (dilution 1:1,000; Santa Cruz Biotchnology, sc-939) to detect endogenous BAG1; (h) rabbit polyclonal Cu/Zn SOD (1:1,000; Enzo Life Science, ADI-SOD-100) to detect SOD1; (i) mouse polyclonal anti-flag M2 (dilution 1:1,000; Sigma-Aldrich, F1804) to detect TARDBP; (j) mouse monoclonal anti-TUBA(dilution 1:4,000; Sigma-Aldrich, T6199); (k) rabbit polyclonal anti-GAPDH (1:4,000; Santa Cruz Biotchnology, sc-25778). Immunoreactivity was detected using the following secondary peroxidase-conjugated antibodies:

goat anti-rabbit (dilution 1:20,000; Santa Cruz Biotchnology, sc-2004); goat anti-mouse (dilution 1:20,000; Santa Cruz Biotchnology, sc-2005). Signals were revealed by chemiluminescence detection kit reagents (Clarity™ Western ECL Blotting Substrate; Bio-Rad, 170-5060). The same membranes were subsequently processed with different antibodies to detect the levels of different proteins in the same sample, after stripping for 20 min at room temperature (StripABlot; Euroclone, EMP100500).

FRA was performed using a Bio-Dot SF Microfiltration Apparatus (Bio-Rad). Six µg of the total SOD1, TARDBP and polyGP proteins or 1.5 µg of the total AR.Q(n) were filtered through a 0.2-µm cellulose acetate membrane (Whatman, 100404180). Slot-blots were probed as described for WB.

A ChemiDoc XRS System (Bio-Rad, Hercules, California, USA) was used for the image acquisition of WB and FRA. Optical density of samples assayed with WB or FRA was detected and analyzed using the Image Lab software (Bio-Rad). Statistical analyses have been performed using the relative optical densities defined as the ratio between optical densities of each independent biological sample (n=3) and the mean optical density of control samples.

Protein Fractionation

Protein fractionation of NSC34 transfected with AR.Q46 was modified from Koyama et al.[143] The cells were harvested and centrifuged 5 min at 100 g at 4°C, then resuspended in PBS containing protease inhibitor cocktail and homogenized using slight sonication. The homogenates were centrifuged at 16,000 g for 10 min at 4°C. Subsequently, the supernatants were collected as the PBS-soluble fraction. The pellets were resuspended in 1% Triton X-100 (TX)-PBS and homogenized using slight sonication. After centrifugation at 16,000 g for 10 min at 4°C, the supernatants were collected as the TX-soluble fraction. Next, the pellets were resuspended in 5% SDS (Fisher Molecular Biology, FS0109)-PBS and homogenized using slight sonication. After centrifugation at 16,000 g for 10 min at 4°C, the supernatants were collected as the SDS-soluble

fraction. Next, the pellets were resuspended in 88% formic acid/PBS and homogenized using slight sonication. After centrifugation at 16,000 g for 10 min at 4°C, the supernatants were collected as the FA-soluble fraction. (See also Fig. S5 in the supplementary materials). Protein concentrations of PBS and TX fractions were measured by a BCA protein assay (Euroclone, EMP014500) and 15 μg were loaded for SDS-polyacrylamide gel electrophoresis. For SDS and FA fractions (10 μL) were loaded for SDS-polyacrylamide gel electrophoresis. All fractions were analyzed as described for WB.

Microscopy analyses on NSC34 cells

NSC34 cells were plated in 12-well multiwell plates containing coverslips at 70,000 cells/well density, transiently transfected with the plasmid coding for AR.Q46 or HSPB8 or with *Dync1h1* siRNA as previously described. AR activation was induced by 10 nM T treatment for 48 h, inhibition of dynein ATPase activity was performed by treatment with 100 μM EHNA for 48 h. In experiments involving autophagy induction, 100 mM trehalose was added to the cells for the last 48 h. Then, the cells were fixed and processed as previously described.[95]

SBMA patient-derived iPSCs cells, differentiated to neuronal cells as described above, were plated in 24-well multiwell plate containing coverslips coated with laminin and poly-D-lysine at 50,000 cell/well density, and allowed to growth and differentiate to motoneuronal cells for 10 days. AR activation was induced by 10 nM T treatment for the last 48 h prior to fixation. Inhibition of dynein ATPase activity was performed by treatment with 100 μM EHNA for the last 48 h prior to fixation. Then the cells were fixed and processed as described previously.[98] The following primary antibodies were used to analyze protein distributions in NSC34: rabbit polyclonal AR-H280 antibody (1:500; Santa Cruz Biotchnology, sc-13062) in TBS-T with 5% nonfat milk, rabbit polyclonal anti-LC3 antibody (1:500, Sigma-Aldrich, L8918) in TBS-T with 5% nonfat milk, and rabbit polyclonal anti-SQSTM1 antibody (1:500; Abcam, ab91526) in TBS-T with 5% nonfat milk. The following primary antibodies were used to analyze protein distributions in differentiated

SBMA patient-derived iPSCs: rabbit polyclonal ARN20 antibody (1:200; Santa Cruz Biotechnology, sc-816) in 3% BSA (Sigma, A7030)-PBS-0.1% Tween 20, mouse monoclonal MNX1/HB9 antibody (1:200; DSHB, 81.5C10) in 3% BSA-PBS-0.1% Tween 20, rabbit polyclonal TUBB3 (1:200; Cell Signaling Technology, 5568) in 3% BSA-PBS-0.1% Tween 20, mouse monoclonal SMI312 antibody (1:1000; Sternberg Monoclonals Incorporated, SMI312) in 3% BSA-PBS-0.1% Tween 20. Secondary antibodies were: Alexa Fluor 488 anti-rabbit (1:1000; Life Technologies, A11070) and Alexa Fluor 594 anti-mouse (1:1000; Life Technologies, A11072) in 3% BSA-PBS-0.1% Tween 20. Cells were stained with DAPI to visualize the nuclei. Images were acquired with i) Axiovert 200 microscope (Zeiss Instr., Oberkochen, Germany) equipped with FITC/TRITC/DAPI filters and combined with a Photometric Cool-Snap CCD camera (Ropper Scientific, Trenton, NJ, USA), phase contrast image was used to evaluate the morphology. Images were processed using the Metamorph software (Universal Imaging, Downingtown, PA, USA). ii) LSM510 Meta system confocal microscope (Zeiss, Oberkochen, Germany) and images were processed with the Aim 4.2 software (Zeiss).

Proteasome activity

Proteasome chymotryptic assay was performed as described by Allen et al.[144] NSC34 cells were plated in 6-well multiwell plates at 180,000 cells/well (4 wells for each condition to be tested; n=4). Where indicated, cells were trasfected with plasmid coding for AR.Q46, as described above, and treated with 10 nM T for 48 h, 100 μM EHNA for 48 h, 10 μM MG132 for the last 16 h, or DMSO for 48 h. Cells were washed with ice-cold PBS and then harvested and centrifuged at 100 x g for 5 min, at 4°C. Pellets resuspended in 0.3 mL of proteasome extract buffer (20 mM Tris HCl, pH 7.4, containing 0.1 mM EDTA, 1 mM 2-mercaptoethanol, 5 mM ATP [Sigma, A1852], 20% v/v glycerol, and 0.04% v/v Nonidet P-40 [Sigma, 98379]) were homogenized by 10 passages through a 21-gauge needle, and then centrifuged at 12,000 x g for 15 min at 4°C, saving the supernatant. Total proteins were determined with BCA protein assay. Proteasome assay reaction mixtures consisted of

50 mM HEPES-KOH, pH 8.0, containing 5 mM EGTA, 100 µg of cell protein extract per mL of assay reaction. Chymotryptic proteasome substrate conjugated with amidomethylcoumarin (AMC), the peptide N-Suc-LLVY-AMC (Sigma, S6510), was added to the mix at 50 µM and incubated at 37°C for 45 min. The resulting fluorescence was measured at 340 nm excitation and 460 nm emission using a plate spectrofluorimeter (Enspire, Perkin Elmer, MA, USA).

Cell viability assay

The 3-(4,5-dimethyl-2-thiazolyl)-2,5 diphenyl-2H-tetrazolium bromide (MTT; Sigma-Aldrich, M2128)-based cell proliferation assay (MTT assay) was carried out on NSC34 cells 24 or 48 h after treatment with 100 µM EHNA, and performed in 24-well multiwell plates at 45,000 cells/well (6 wells for each condition to be tested; n=6). MTT solution was prepared at 1.5 mg/mL in DMEM without phenol red and was filtered through a 0.2-µm filter. Then, the culture medium was removed from the plate and 300 µL of MTT solution was added into each well. Cells were incubated for 30 min at 37°C with 5% CO_2, 95% air and complete humidity. After 30 min, 500 µL of 2-propanol was added into each well and the precipitates were suspended. The optical density (OD) of the wells was determined using a plate reader at a wavelength of 550 nm.

β-galactosidase assay

NSC34 cells were plated in 24-well multiwell plates at density of 40,000 cells/well (6 wells for each condition to be tested; n=6) and transfected with 0.4 µg of pCMV-βgal plasmid. 24 h after transfection the cells were lysed in 250 µL of lysis buffer (Promega, E194A) and 100 µL of samples were added to 750 µL of assay buffer (60 mM Na_2HPO_4 40 mM NaH_2PO_4 10 mM KCl, 1 mM $MgSO_4$, 50 mM β-mercaptoethanol, pH 7.0), in presence of 4 mg/mL of β-galactosidase substrate o-nitrophenyl-β-D-galactopyraniside (ONPG; Sigma-Aldrich, N1127) and incubated at 37°C until yellow color appearance. Then, 500 µL of 1M Na_2CO_3 were added and 200 µL of the

final solution were transferred into a 96-well plate and 420-nm absorbance was evaluated using Enspire plate spectrofluorimeter (PerkinElmer).

Statistical analysis

In all figures, data are presented as mean ± SD. Statistical analysis has been performed by using the one-tailed unpaired Student t test to compare data between 2 groups, One-Way ANOVA to compare more than 2 groups of data, and Two-Way ANOVA to compare the effect of 2 different independent variables (see figure legends for details). When ANOVA resulted to be significant, we performed an Uncorrected Fisher LSD *post hoc* test (and the one-tailed unpaired Student t test when the variances between groups were highly different) (see figure legends for details) for multiple comparisons. Computations were done with the PRISM (ver. 6.0h) software (GraphPad Software, La Jolla, CA, USA).

ABBREVIATIONS

3MA	3-methyladenine
ALS	amyotrophic lateral sclerosis
AR	androgen receptor
BAG1	BCL2-associated athanogene 1
BAG3	BCL2-associated athanogene 3
C9ORF72	chromosome 9 open reading frame 72
CMA	chaperone-mediated autophagy
DYNC1H1	dynein cytoplasmic 1 heavy chain 1
EHNA	erythro-9-[3-2-(hydrosynony)] adenine
FA	formic acid
FALS	familial ALS
FRA	filter-retardation assay
GAPDH	glyceraldheyde-3-phosphate dehydrogenase
GP	dipeptide (glycine-proline)
HDAC6	histone deacetylase 6
HSP	heat shock protein
HSPA	heat shock protein A
HSPA1A	heat shock protein 1A
HSPA8/HSC70	heat shock protein 8
HSPB8	small heat shock protein 8
IF	immunofluorescence analysis
IPSCS	induced pluripotent stem cells
MAP1LC3/LC3	microtuble-associated protein 1 light chain 3
MNDS	motoneuron diseases
MNX1/HB9	motor neuron and pancreas homeobox 1

MTOC	microtubule-organization centre
ND	neurodegenerative disease
PQC	protein quality control
SALS	sporadic ALS
SBMA	spinal bulbar muscular atrophy
SOD1	superoxide dismutase 1, soluble
SQSTM1/p62	sequestosome 1
STUB1/CHIP	stip1 homology and u-box containing protein 1
T	testosterone
TARDBP/TDP-43	tar dna binding protein
TFEB	transcription factor eB
TUBA/α-TUBULIN	tubulin, alpha
TUBB3/βIII-TUBULIN	tubulin, beta 3 class III
UPS	ubiquitin-proteasome systEM
WB	western blot
WT	wild type

Acknowledgements: The following grants are gratefully acknowledged: Fondazione Telethon, Italy (n. GGP14039 to A.P.); Fondazione Cariplo, Italy (n. 2014-0686 to A.P. and S.C.); Fondazione AriSLA, Italy (n. ALS_HSPB8 to A.P. and S.C.; ALS_Granulopathy to A.P. and S.C.); Association Française contre les Myopathies, France (AFM Telethon n. 16406 to A.P.); Regione Lombardia (to A.P.); Università degli Studi di Milano e piano di sviluppo UNIMI - linea B (to P.R.); Italian Ministry of Health (MinSal) (n. GR-2011-02347198 to V.C. and S.C.); Joint Programme on Neurodegenerative Diseases (JPND, CureALS), EC (to A.P. and S.C.); Fondazione regionale per la ricerca biomedica (FRRB) (TRANS_ALS), Regione Lombardia, Italy (to A.P.); MIUR Rita Levi Montalcini (to S.C.); Italian Ministry of University and Research (MIUR), PRIN - Progetti di ricerca di interesse nazionale (n. 2015LFPNMN to A.P. and S.C.); European Molecular Biology Organization (EMBO), short term fellowship (n. 537 - 2015 to R.C.)

The authors are grateful to Dr. Kennet Fischbeck (NINDS-NIH, Bethesta, USA) for having provided the iPSCs derived fibroblast of SBMA patients and controls; to Dr. Enrico Garattini (Mario Negri Institute, Milan, Italy) for TR4 NSC34 cells; to Prof. D. Ito (Department of Neurology, Keio University School of Medicine, Tokyo, Japan) for the pCMV-Flag-polyGP-V5-His encoding the poly-GP; to Prof E. Buratti (International Centre for Genetic Engineering and Biotechnology, Trieste, Italy) for the pFLAG-FL TDP-43, and pFLAG-ΔC TDP-43; to Prof. Diane Merry Merry (Thomas Jefferson University, Philadelphia, PA, USA) for the PC12-AR.Q112; to Prof. R. Kopito (Stanford University, Stanford, CA, USA) for the reporter plasmid GFPu; to Prof. H.H. Kampinga (University of Groningen, Groningen, The Netherlands) for the pcDNA/HA-Bag1; to Dr. A. Boncoraglio for the fruitful discussion.

REFERENCES

1. Cleveland DW, Rothstein JD. From Charcot to Lou Gehrig: deciphering selective motor neuron death in ALS. Nat Rev Neurosci 2001; 2:806-19. doi:10.1038/35097565
2. Boillée S, Vande Velde C, Cleveland DW. ALS: a disease of motor neurons and their nonneuronal neighbors. Neuron 2006; 52:39-59. doi:10.1016/j.neuron.2006.09.018
3. Lobsiger CS, Boillee S, McAlonis-Downes M, Khan AM, Feltri ML, Yamanaka K, Cleveland DW. Schwann cells expressing dismutase active mutant SOD1 unexpectedly slow disease progression in ALS mice. Proc Natl Acad Sci U S A 2009; 106:4465-70. doi:10.1073/pnas.0813339106
4. Cortes CJ, Ling SC, Guo LT, Hung G, Tsunemi T, Ly L, Tokunaga S, Lopez E, Sopher BL, Bennett CF, et al. Muscle expression of mutant androgen receptor accounts for systemic and motor neuron disease phenotypes in spinal and bulbar muscular atrophy. Neuron 2014; 82:295-307. doi:10.1016/j.neuron.2014.03.001
5. Lieberman AP, Yu Z, Murray S, Peralta R, Low A, Guo S, Yu XX, Cortes CJ, Bennett CF, Monia BP, et al. Peripheral androgen receptor gene suppression rescues disease in mouse models of spinal and bulbar muscular atrophy. Cell Rep 2014; 7:774-84. doi:10.1016/j.celrep.2014.02.008
6. Dobrowolny G, Aucello M, Rizzuto E, Beccafico S, Mammucari C, Bonconpagni S, Belia S, Wannenes F, Nicoletti C, Del Prete Z, et al. Skeletal muscle is a primary target of SOD1G93A-mediated toxicity. Cell Metab 2008; 8:425-36. doi:10.1016/j.cmet.2008.09.002
7. Halievski K, Henley CL, Domino L, Poort JE, Fu M, Katsuno M, Adachi H, Sobue G, Breedlove SM, Jordan CL. Androgen-dependent loss of muscle BDNF mRNA in two mouse models of SBMA. Exp Neurol 2015. doi:10.1016/j.expneurol.2015.04.013
8. Monks DA, Johansen JA, Mo K, Rao P, Eagleson B, Yu Z, Lieberman AP, Breedlove SM, Jordan CL. Overexpression of wild-type androgen receptor in muscle recapitulates polyglutamine disease. Proc Natl Acad Sci U S A 2007; 104:18259-64. doi:10.1073/pnas.0705501104
9. Jordan CL, Lieberman AP. Spinal and bulbar muscular atrophy: a motoneuron or muscle disease? Curr Opin Pharmacol 2008; 8:752-8. doi:10.1016/j.coph.2008.08.006
10. Johansen JA, Yu Z, Mo K, Monks DA, Lieberman AP, Breedlove SM, Jordan CL. Recovery of function in a myogenic mouse model of spinal bulbar muscular atrophy. Neurobiol Dis 2009; 34:113-20. doi:10.1016/j.nbd.2008.12.009
11. Oki K, Wiseman RW, Breedlove SM, Jordan CL. Androgen receptors in muscle fibers induce rapid loss of force but not mass: implications for spinal bulbar muscular atrophy. Muscle Nerve 2013; 47:823-34. doi:10.1002/mus.23813
12. Galbiati M, Crippa V, Rusmini P, Cristofani R, Cicardi ME, Giorgetti E, Onesto E, Messi E, Poletti A. ALS-related misfolded protein management in motor neurons and muscle cells. Neurochem Int 2014; 79:70-8. doi:10.1016/j.neuint.2014.10.007
13. Baralle M, Buratti E, Baralle FE. The role of TDP-43 in the pathogenesis of ALS and FTLD. Biochem Soc Trans 2013; 41:1536-40. doi:10.1042/BST20130186
14. Cozzolino M, Pesaresi MG, Gerbino V, Grosskreutz J, Carri MT. Amyotrophic lateral sclerosis: new insights into underlying molecular mechanisms and opportunities for therapeutic intervention. Antioxid Redox Signal 2012; 17:1277-330. doi:10.1089/ars.2011.4328
15. Ciechanover A, Kwon YT. Degradation of misfolded proteins in neurodegenerative diseases: therapeutic targets and strategies. Exp Mol Med 2015; 47:e147. doi:10.1038/emm.2014.117

16. La Spada AR, Wilson EM, Lubahn DB, Harding AE, Fischbeck KH. Androgen receptor gene mutations in X-linked spinal and bulbar muscular atrophy. Nature 1991; 352:77-9. doi:10.1038/352077a0
17. Katsuno M, Adachi H, Kume A, Li M, Nakagomi Y, Niwa H, Sang C, Kobayashi Y, Doyu M, Sobue G. Testosterone reduction prevents phenotypic expression in a transgenic mouse model of spinal and bulbar muscular atrophy. Neuron 2002; 35:843-54. doi:10.1016/S0896-6273(02)00834-6
18. Poletti A. The polyglutamine tract of androgen receptor: from functions to dysfunctions in motor neurons. Front Neuroendocrinol 2004; 25:1-26. doi:10.1016/j.yfrne.2004.03.001
19. Robberecht W, Philips T. The changing scene of amyotrophic lateral sclerosis. Nat Rev Neurosci 2013; 14:248-64. doi:10.1038/nrn3430
20. Simeoni S, Mancini MA, Stenoien DL, Marcelli M, Weigel NL, Zanisi M, Martini L, Poletti A. Motoneuronal cell death is not correlated with aggregate formation of androgen receptors containing an elongated polyglutamine tract. Hum Mol Genet 2000; 9:133-44. doi:10.1093/hmg/9.1.133
21. Saudou F, Finkbeiner S, Devys D, Greenberg ME. Huntingtin acts in the nucleus to induce apoptosis but death does not correlate with the formation of intranuclear inclusions. Cell 1998; 95:55-66. doi:10.1016/S0092-8674(00)81782-1
22. Klement IA, Skinner PJ, Kaytor MD, Yi H, Hersch SM, Clark HB, Zoghbi HY, Orr HT. Ataxin-1 nuclear localization and aggregation - role in polyglutamine-induced disease in SCA1 transgenic mice. Cell 1998; 95:41-53. doi:10.1016/S0092-8674(00)81781-X
23. Arrasate M, Mitra S, Schweitzer ES, Segal MR, Finkbeiner S. Inclusion body formation reduces levels of mutant huntingtin and the risk of neuronal death. Nature 2004; 431:805-10. doi:10.1038/nature02998
24. Montie HL, Cho MS, Holder L, Liu Y, Tsvetkov AS, Finkbeiner S, Merry DE. Cytoplasmic retention of polyglutamine-expanded androgen receptor ameliorates disease via autophagy in a mouse model of spinal and bulbar muscular atrophy. Hum Mol Genet 2009; 18:1937-50. doi:10.1093/hmg/ddp115
25. Piccioni F, Pinton P, Simeoni S, Pozzi P, Fascio U, Vismara G, Martini L, Rizzuto R, Poletti A. Androgen receptor with elongated polyglutamine tract forms aggregates that alter axonal trafficking and mitochondrial distribution in motor neuronal processes. Faseb J 2002; 16:1418-20. doi:10.1096/fj.01-1035fje
26. Johnston JA, Illing ME, Kopito RR. Cytoplasmic dynein/dynactin mediates the assembly of aggresomes. Cell motil cytoskeleton 2002; 53:26-38. doi:10.1002/cm.10057
27. Carra S, Crippa V, Rusmini P, Boncoraglio A, Minoia M, Giorgetti E, Kampinga HH, Poletti A. Alteration of protein folding and degradation in motor neuron diseases: Implications and protective functions of small heat shock proteins. Prog Neurobiol 2012; 97:83-100. doi:10.1016/j.pneurobio.2011.09.009
28. Crippa V, Carra S, Rusmini P, Sau D, Bolzoni E, Bendotti C, De Biasi S, Poletti A. A role of small heat shock protein B8 (HspB8) in the autophagic removal of misfolded proteins responsible for neurodegenerative diseases. Autophagy 2010; 6:958-60. doi:10.4161/auto.6.7.13042
29. Crippa V, Sau D, Rusmini P, Boncoraglio A, Onesto E, Bolzoni E, Galbiati M, Fontana E, Marino M, Carra S, et al. The small heat shock protein B8 (HspB8) promotes autophagic removal of misfolded proteins involved in amyotrophic lateral sclerosis (ALS). Hum Mol Genet 2010; 19:3440-56. doi:10.1093/hmg/ddq257
30. Carra S, Sivilotti M, Chavez Zobel AT, Lambert H, Landry J. HspB8, a small heat shock protein mutated in human neuromuscular disorders, has in vivo chaperone activity in cultured cells. Hum Mol Genet 2005; 14:1659-69. doi: 10.1093/hmg/ddi174
31. Giorgetti E, Rusmini P, Crippa V, Cristofani R, Boncoraglio A, Cicardi ME, Galbiati M, Poletti A. Synergic prodegradative activity of Bicalutamide and trehalose on the mutant

androgen receptor responsible for spinal and bulbar muscular atrophy. Hum Mol Genet 2015; 24:64-75. doi:10.1093/hmg/ddu419
32. Rusmini P, Crippa V, Giorgetti E, Boncoraglio A, Cristofani R, Carra S, Poletti A. Clearance of the mutant androgen receptor in motoneuronal models of spinal and bulbar muscular atrophy. Neurobiol Aging 2013; 34:2585-603. doi:10.1016/j.neurobiolaging.2013.05.026
33. Crippa V, D'Agostino VG, Cristofani R, Rusmini P, Cicardi ME, Messi E, et al. Transcriptional induction of the heat shock protein B8 mediates the clearance of misfolded proteins responsible for motor neuron diseases. Sci Rep 2016; 6:22827. doi:10.1038/srep22827
34. Carra S, Seguin SJ, Landry J. HspB8 and Bag3: a new chaperone complex targeting misfolded proteins to macroautophagy. Autophagy 2008; 4:237-9. doi:10.4161/auto.5407
35. Carra S. The stress-inducible HspB8-Bag3 complex induces the eIF2alpha kinase pathway: implications for protein quality control and viral factory degradation? Autophagy 2009; 5:428-9. doi:10.4161/auto.5.3.7894
36. Gamerdinger M, Carra S, Behl C. Emerging roles of molecular chaperones and co-chaperones in selective autophagy: focus on BAG proteins. J Mol Med (Berl) 2011; 89:1175-82. doi:10.1007/s00109-011-0795-6
37. Takayama S, Reed JC. Molecular chaperone targeting and regulation by BAG family proteins. Nat cell biol 2001; 3:E237-41. doi:10.1038/ncb1001-e237
38. Minoia M, Boncoraglio A, Vinet J, Morelli FF, Brunsting JF, Poletti A, Krom S, Reits E, Kampinga HH, Carra S. BAG3 induces the sequestration of proteasomal clients into cytoplasmic puncta: Implications for a proteasome-to-autophagy switch. Autophagy 2014; 10. doi: 10.4161/auto.29409
39. Arndt V, Dick N, Tawo R, Dreiseidler M, Wenzel D, Hesse M, Furst DO, Saftig P, Saint R, Fleischmann BK, et al. Chaperone-assisted selective autophagy is essential for muscle maintenance. Curr Biol 2010; 20:143-8. doi:10.1016/j.cub.2009.11.022
40. Klionsky DJ, Abdelmohsen K, Abe A, Abedin MJ, Abeliovich H, Acevedo Arozena A, Adachi H, Adams CM, Adams PD, Adeli K, et al. Guidelines for the use and interpretation of assays for monitoring autophagy (3rd edition). Autophagy 2016; 12:1-222. doi:10.1080/15548627.2015.1100356
41. Fuchs M, Poirier DJ, Seguin SJ, Lambert H, Carra S, Charette SJ, Landry J. Identification of the key structural motifs involved in HspB8/HspB6-Bag3 interaction. Biochem J 2010; 425:245-55. doi:10.1042/BJ20090907
42. Gamerdinger M, Kaya AM, Wolfrum U, Clement AM, Behl C. BAG3 mediates chaperone-based aggresome-targeting and selective autophagy of misfolded proteins. EMBO Rep 2011; 12:149-56. doi:10.1038/embor.2010.203
43. Behl C. BAG3 and friends: co-chaperones in selective autophagy during aging and disease. Autophagy 2011; 7:795-8. doi:10.4161/auto.7.7.15844
44. Sondermann H, Scheufler C, Schneider C, Hohfeld J, Hartl FU, Moarefi I. Structure of a Bag/Hsc70 complex: convergent functional evolution of Hsp70 nucleotide exchange factors. Science 2001; 291:1553-7. doi:10.1126/science.291.5508.1553
45. Rauch JN, Gestwicki JE. Binding of human nucleotide exchange factors to heat shock protein 70 (Hsp70) generates functionally distinct complexes in vitro. J Biol Chem 2014; 289:1402-14. doi:10.1074/jbc.M113.521997
46. Garcia-Mata R, Bebok Z, Sorscher EJ, Sztul ES. Characterization and dynamics of aggresome formation by a cytosolic GFP-chimera. J Cell Biol 1999; 146:1239-54. doi:10.1083/jcb.146.6.1239
47. Kawaguchi Y, Kovacs JJ, McLaurin A, Vance JM, Ito A, Yao TP. The deacetylase HDAC6 regulates aggresome formation and cell viability in response to misfolded protein stress. Cell 2003; 115:727-38. doi:10.1016/S0092-8674(03)00939-5

48. Iwata A, Riley BE, Johnston JA, Kopito RR. HDAC6 and Microtubules Are Required for Autophagic Degradation of Aggregated Huntingtin. J Biol Chem 2005; 280:40282-92. doi:10.1074/jbc.M508786200
49. Dompierre JP, Godin JD, Charrin BC, Cordelieres FP, King SJ, Humbert S, Saudou F. Histone deacetylase 6 inhibition compensates for the transport deficit in Huntington's disease by increasing tubulin acetylation. J Neurosci 2007; 27:3571-83. doi:10.1523/JNEUROSCI.0037-07.2007
50. Pandey UB, Nie Z, Batlevi Y, McCray BA, Ritson GP, Nedelsky NB, Schwartz SL, DiProspero NA, Knight MA, Schuldiner O, et al. HDAC6 rescues neurodegeneration and provides an essential link between autophagy and the UPS. Nature 2007; 447:859-63. doi:10.1038/nature05853
51. Lee JY, Koga H, Kawaguchi Y, Tang W, Wong E, Gao YS, Pandey UB, Kaushik S, Tresse E, Lu J, et al. HDAC6 controls autophagosome maturation essential for ubiquitin-selective quality-control autophagy. EMBO J 2010; 29:969-80. doi:10.1038/emboj.2009.405
52. Munoz-Moreno R, Barrado-Gil L, Galindo I, Alonso C. Analysis of HDAC6 and BAG3-aggresome pathways in African swine fever viral factory formation. Viruses 2015; 7:1823-31. doi:10.3390/v7041823
53. Sha Y, Pandit L, Zeng S, Eissa NT. A critical role for CHIP in the aggresome pathway. Mol Cell Biol 2009; 29:116-28. doi:10.1128/MCB.00829-08
54. Kraft C, Peter M, Hofmann K. Selective autophagy: ubiquitin-mediated recognition and beyond. Nat Cell Biol 2010; 12:836-41. doi:10.1038/ncb0910-836
55. Weedon MN, Hastings R, Caswell R, Xie W, Paszkiewicz K, Antoniadi T, Williams M, King C, Greenhalgh L, Newbury-Ecob R, et al. Exome sequencing identifies a DYNC1H1 mutation in a large pedigree with dominant axonal Charcot-Marie-Tooth disease. Am J Hum Genet 2011; 89:308-12. doi:10.1016/j.ajhg.2011.07.002
56. Harms MB, Ori-McKenney KM, Scoto M, Tuck EP, Bell S, Ma D, Masi S, Allred P, Al-Lozi M, Reilly MM, et al. Mutations in the tail domain of DYNC1H1 cause dominant spinal muscular atrophy. Neurology 2012; 78:1714-20. doi:10.1212/WNL.0b013e3182556c05
57. Strickland AV, Schabhuttl M, Offenbacher H, Synofzik M, Hauser NS, Brunner-Krainz M, Gruber-Sedlmayr U, Moore SA, Windhager R, Bender B, et al. Mutation screen reveals novel variants and expands the phenotypes associated with DYNC1H1. J Neurol 2015. doi:10.1007/s00415-015-7727-2
58. Scoto M, Rossor AM, Harms MB, Cirak S, Calissano M, Robb S, Manzur AY, Martinez Arroyo A, Rodriguez Sanz A, Mansour S, et al. Novel mutations expand the clinical spectrum of DYNC1H1-associated spinal muscular atrophy. Neurology 2015; 84:668-79. doi:10.1212/WNL.0000000000001269
59. LaMonte BH, Wallace KE, Holloway BA, Shelly SS, Ascano J, Tokito M, Van Winkle T, Howland DS, Holzbaur EL. Disruption of dynein/dynactin inhibits axonal transport in motor neurons causing late-onset progressive degeneration. Neuron 2002; 34:715-27. doi:10.1016/S0896-6273(02)00696-7
60. Hafezparast M, Klocke R, Ruhrberg C, Marquardt A, Ahmad-Annuar A, Bowen S, Lalli G, Witherden AS, Hummerich H, Nicholson S, et al. Mutations in dynein link motor neuron degeneration to defects in retrograde transport. Science 2003; 300:808-12. doi:10.1126/science.1083129
61. Ravikumar B, Acevedo-Arozena A, Imarisio S, Berger Z, Vacher C, O'Kane CJ, Brown SD, Rubinsztein DC. Dynein mutations impair autophagic clearance of aggregate-prone proteins. Nat Genet 2005; 37:771-6. doi:10.1038/ng1591
62. Sau D, Rusmini P, Crippa V, Onesto E, Bolzoni E, Ratti A, Poletti A. Dysregulation of axonal transport and motorneuron diseases. Biol Cell 2011; 103:87-107. doi:10.1042/BC20100093

63. Teuchert M, Fischer D, Schwalenstoecker B, Habisch HJ, Bockers TM, Ludolph AC. A dynein mutation attenuates motor neuron degeneration in SOD1(G93A) mice. Exp Neurol 2006; 198:271-4. doi:10.1016/j.expneurol.2005.12.005
64. Zhang F, Strom A-L, Fukada K, Lee S, Hayward LJ, Zhu H. Interaction between Familial Amyotrophic Lateral Sclerosis (ALS)-linked SOD1 Mutants and the Dynein Complex. J Biol Chem 2007; 282:16691-9. doi:10.1074/jbc.M609743200
65. El-Kadi AM, Bros-Facer V, Deng W, Philpott A, Stoddart E, Banks G, Jackson GS, Fisher EM, Duchen MR, Greensmith L, et al. The Legs at odd angles (Loa) mutation in cytoplasmic dynein ameliorates mitochondrial function in SOD1G93A mouse model for motor neuron disease. J Biol Chem 2010; 285:18627-39. doi:10.1074/jbc.M110.129320
66. Behl C. Breaking BAG: The Co-Chaperone BAG3 in Health and Disease. Trends Pharmacol Sci 2016. doi:10.1016/j.tips.2016.04.007
67. Nollen EA, Kabakov AE, Brunsting JF, Kanon B, Hohfeld J, Kampinga HH. Modulation of in vivo HSP70 chaperone activity by Hip and Bag-1. J Biol Chem 2001; 276:4677-82. doi: 10.1074/jbc.M009745200
68. Stenoien DL, Cummings CJ, Adams HP, Mancini MG, Patel K, DeMartino G, Marcelli M, Weigel NL, Mancini MA. Polyglutamine-expanded androgen receptors form aggregates that sequester heat shock proteins, proteasome components and SRC-1, and are suppressed by the HDJ-2 chaperone. Hum Mol Genet 1999; 8:731-41. doi:10.1093/hmg/8.5.731
69. Rusmini P, Simonini F, Crippa V, Bolzoni E, Onesto E, Cagnin M, Sau D, Ferri N, Poletti A. 17-AAG increases autophagic removal of mutant androgen receptor in spinal and bulbar muscular atrophy. Neurobiol Dis 2011; 41:83-95. doi:10.1016/j.nbd.2010.08.023
70. Carra S, Seguin SJ, Lambert H, Landry J. HspB8 chaperone activity toward poly(Q)-containing proteins depends on its association with Bag3, a stimulator of macroautophagy. J Biol Chem 2008; 283:1437-44. doi:10.1074/jbc.M706304200
71. Strong MJ. The evidence for altered RNA metabolism in amyotrophic lateral sclerosis (ALS). J Neurol Sci 2010; 288:1-12. doi:10.1016/j.jns.2009.09.029
72. Volkening K, Leystra-Lantz C, Yang W, Jaffee H, Strong MJ. Tar DNA binding protein of 43 kDa (TDP-43), 14-3-3 proteins and copper/zinc superoxide dismutase (SOD1) interact to modulate NFL mRNA stability. Implications for altered RNA processing in amyotrophic lateral sclerosis (ALS). Brain Res 2009; 1305:168-82. doi:10.1016/j.brainres.2009.09.105
73. Xu Z, Graham K, Foote M, Liang F, Rizkallah R, Hurt M, Wang Y, Wu Y, Zhou Y. 14-3-3 protein targets misfolded chaperone-associated proteins to aggresomes. J Cell Sci 2013; 126:4173-86. doi:10.1242/jcs.126102
74. Jia B, Wu Y, Zhou Y. 14-3-3 and aggresome formation: implications in neurodegenerative diseases. Prion 2014; 8. doi:10.4161/pri.28123
75. Gennerich A, Carter AP, Reck-Peterson SL, Vale RD. Force-induced bidirectional stepping of cytoplasmic dynein. Cell 2007; 131:952-65. doi:10.1016/j.cell.2007.10.016
76. Penningroth SM, Cheung A, Bouchard P, Gagnon C, Bardin CW. Dynein ATPase is inhibited selectively in vitro by erythro-9-[3-2-(hydroxynonyl)]adenine. Biochem Biophys Res Commun 1982; 104:234-40. doi:10.1016/0006-291X(82)91964-7
77. Kaplan A, Reiner O. Linking cytoplasmic dynein and transport of Rab8 vesicles to the midbody during cytokinesis by the doublecortin domain-containing 5 protein. J Cell Sci 2011; 124:3989-4000. doi:10.1242/jcs.085407
78. Tanaka M, Machida Y, Niu S, Ikeda T, Jana NR, Doi H, Kurosawa M, Nekooki M, Nukina N. Trehalose alleviates polyglutamine-mediated pathology in a mouse model of Huntington disease. Nat Med 2004; 10:148-54. doi:10.1038/nm985
79. Sarkar S, Davies JE, Huang Z, Tunnacliffe A, Rubinsztein DC. Trehalose, a novel mTOR-independent autophagy enhancer, accelerates the clearance of mutant huntingtin and alpha-synuclein. J Biol Chem 2007; 282:5641-52. doi:10.1074/jbc.M609532200

80. Zhang X, Chen S, Song L, Tang Y, Shen Y, Jia L, Le W. MTOR-independent, autophagic enhancer trehalose prolongs motor neuron survival and ameliorates the autophagic flux defect in a mouse model of amyotrophic lateral sclerosis. Autophagy 2014; 10. doi:10.4161/auto.27710
81. Berger TR, Montie HL, Jain P, Legleiter J, Merry DE. Identification of novel polyglutamine-expanded aggregation species in spinal and bulbar muscular atrophy. Brain Res 2015; 1628:254-64. doi:10.1016/j.brainres.2015.09.033
82. Heine EM, Berger TR, Pluciennik A, Orr CR, Merry DE. Proteasome-Mediated Proteolysis of the Polyglutamine-Expanded Androgen Receptor is a Late Event in SBMA Pathogenesis. J Biol Chem 2015. doi:10.1074/jbc.M114.617894
83. Zboray L, Pluciennik A, Curtis D, Liu Y, Berman-Booty LD, Orr C, Kesler CT, Berger T, Gioeli D, Paschal BM, et al. Preventing the Androgen Receptor N/C Interaction Delays Disease Onset in a Mouse Model of SBMA. Cell Rep 2015; 13:2312-23. doi:10.1016/j.celrep.2015.11.019
84. Chua JP, Reddy SL, Yu Z, Giorgetti E, Montie HL, Mukherjee S, Higgins J, McEachin RC, Robins DM, Merry DE, et al. Disrupting SUMOylation enhances transcriptional function and ameliorates polyglutamine androgen receptor-mediated disease. J Clin Invest 2015; 125:831-45. doi:10.1172/JCI73214
85. Palazzolo I, Nedelsky NB, Askew CE, Harmison GG, Kasantsev AG, Taylor JP, Fischbeck KH, Pennuto M. B2 attenuates polyglutamine-expanded androgen receptor toxicity in cell and fly models of spinal and bulbar muscular atrophy. J Neurosci Res 2010; 88:2207-16. doi:10.1002/jnr.22389
86. Rusmini P, Sau D, Crippa V, Palazzolo I, Simonini F, Onesto E, Martini L, Poletti A. Aggregation and proteasome: the case of elongated polyglutamine aggregation in spinal and bulbar muscular atrophy. Neurobiol Aging 2007; 28:1099-111. doi:10.1016/j.neurobiolaging.2006.05.015
87. Rusmini P, Bolzoni E, Crippa V, Onesto E, Sau D, Galbiati M, Piccolella M, Poletti A. Proteasomal and autophagic degradative activities in spinal and bulbar muscular atrophy. Neurobiol Dis 2010; 40:361-9. doi:10.1016/j.nbd.2010.06.016
88. Dossena M, Bedini G, Rusmini P, Giorgetti E, Canazza A, Tosetti V, Salsano E, Sagnelli A, Mariotti C, Gellera C, et al. Human adipose-derived mesenchymal stem cells as a new model of spinal and bulbar muscular atrophy. PLoS One 2014; 9:e112746. doi:10.1371/journal.pone.0112746
89. Walcott JL, Merry DE. Ligand promotes intranuclear inclusions in a novel cell model of spinal and bulbar muscular atrophy. J Biol Chem 2002; 277:50855-9. doi:10.1074/jbc.M209466200
90. Montie HL, Merry DE. Autophagy and access: understanding the role of androgen receptor subcellular localization in SBMA. Autophagy 2009; 5:1194-7. doi:10.4161/auto.5.8.9726
91. Fischbeck KH. Kennedy disease. J Inher Metab Dis 1997; 20:152-8. doi:10.1023/A:1005344403603
92. Rhodes LE, Freeman BK, Auh S, Kokkinis AD, La Pean A, Chen C, Lehky TJ, Shrader JA, Levy EW, Harris-Love M, et al. Clinical features of spinal and bulbar muscular atrophy. Brain 2009; 132:3242-51. doi:10.1093/brain/awp258
93. Grunseich C, Rinaldi C, Fischbeck KH. Spinal and bulbar muscular atrophy: pathogenesis and clinical management. Oral Dis 2014; 20:6-9. doi:10.1093/brain/awp258
94. Bence NF, Sampat RM, Kopito RR. Impairment of the ubiquitin-proteasome system by protein aggregation. Science 2001; 292:1552-5. doi:10.1126/science.292.5521.1552
95. Sau D, De Biasi S, Vitellaro-Zuccarello L, Riso P, Guarnieri S, Porrini M, Simeoni S, Crippa V, Onesto E, Palazzolo I, et al. Mutation of SOD1 in ALS: a gain of a loss of function. Hum Mol Genet 2007; 16:1604-18. doi:10.1093/hmg/ddm110

96. Carra S, Rusmini P, Crippa V, Giorgetti E, Boncoraglio A, Cristofani R, Naujock M, Meister M, Minoia M, Kampinga HH, et al. Different anti-aggregation and pro-degradative functions of the members of the mammalian sHSP family in neurological disorders. Philos Trans R Soc Lond B Biol Sci 2013; 368:20110409. doi:10.1098/rstb.2011.0409
97. Luders J, Demand J, Hohfeld J. The ubiquitin-related BAG-1 provides a link between the molecular chaperones Hsc70/Hsp70 and the proteasome. J Biol Chem 2000; 275:4613-7. doi:10.1074/jbc.275.7.4613
98. Grunseich C, Zukosky K, Kats IR, Ghosh L, Harmison GG, Bott LC, Rinaldi C, Chen KL, Chen G, Boehm M, et al. Stem cell-derived motor neurons from spinal and bulbar muscular atrophy patients. Neurobiol Dis 2014; 70:12-20. doi:10.1016/j.nbd.2014.05.038
99. Bendotti C, Marino M, Cheroni C, Fontana E, Crippa V, Poletti A, De Biasi S. Dysfunction of constitutive and inducible ubiquitin-proteasome system in amyotrophic lateral sclerosis: implication for protein aggregation and immune response. Prog Neurobiol 2012; 97:101-26. doi:10.1016/j.pneurobio.2011.10.001
100. Al-Sarraj S, King A, Troakes C, Smith B, Maekawa S, Bodi I, Rogelj B, Al-Chalabi A, Hortobagyi T, Shaw CE. p62 positive, TDP-43 negative, neuronal cytoplasmic and intranuclear inclusions in the cerebellum and hippocampus define the pathology of C9orf72-linked FTLD and MND/ALS. Acta Neuropathol 2011; 122:691-702. doi:10.1007/s00401-011-0911-2
101. DeJesus-Hernandez M, Mackenzie IR, Boeve BF, Boxer AL, Baker M, Rutherford NJ, Nicholson AM, Finch NA, Flynn H, Adamson J, et al. Expanded GGGGCC hexanucleotide repeat in noncoding region of C9ORF72 causes chromosome 9p-linked FTD and ALS. Neuron 2011; 72:245-56. doi:10.1016/j.neuron.2011.09.011
102. Renton AE, Majounie E, Waite A, Simon-Sanchez J, Rollinson S, Gibbs JR, Schymick JC, Laaksovirta H, van Swieten JC, Myllykangas L, et al. A hexanucleotide repeat expansion in C9ORF72 is the cause of chromosome 9p21-linked ALS-FTD. Neuron 2011; 72:257-68. doi:10.1016/j.neuron.2011.09.010
103. Brettschneider J, Van Deerlin VM, Robinson JL, Kwong L, Lee EB, Ali YO, Safren N, Monteiro MJ, Toledo JB, Elman L, et al. Pattern of ubiquilin pathology in ALS and FTLD indicates presence of C9ORF72 hexanucleotide expansion. Acta Neuropathol 2012; 123:825-39. doi:10.1007/s00401-012-0970-z
104. Ash PE, Bieniek KF, Gendron TF, Caulfield T, Lin WL, Dejesus-Hernandez M, van Blitterswijk MM, Jansen-West K, Paul JW, 3rd, Rademakers R, et al. Unconventional Translation of C9ORF72 GGGGCC Expansion Generates Insoluble Polypeptides Specific to c9FTD/ALS. Neuron 2013; 77:639-46. doi:10.1016/j.neuron.2013.02.004
105. Cleary JD, Ranum LP. Repeat-associated non-ATG (RAN) translation in neurological disease. Hum Mol Genet 2013. doi:10.1093/hmg/ddt371
106. Lashley T, Hardy J, Isaacs AM. RANTing about C9orf72. Neuron 2013; 77:597-8. doi:10.1016/j.neuron.2013.02.009
107. Yamakawa M, Ito D, Honda T, Kubo K, Noda M, Nakajima K, Suzuki N. Characterization of the dipeptide repeat protein in the molecular pathogenesis of c9FTD/ALS. Hum Mol Genet 2015; 24:1630-45. doi:10.1093/hmg/ddu576
108. Alexandrova A, Petrov L, Georgieva A, Kirkova M, Kukan M. Effects of proteasome inhibitor, MG132, on proteasome activity and oxidative status of rat liver. Cell Biochem Funct 2008; 26:392-8. doi:10.1002/cbf.1459
109. Onesto E, Rusmini P, Crippa V, Ferri N, Zito A, Galbiati M, Poletti A. Muscle cells and motoneurons differentially remove mutant SOD1 causing familial amyotrophic lateral sclerosis. J Neurochem 2011; 118:266-80. doi:10.1111/j.1471-4159.2011.07298.x
110. Rohde G, Kermer P, Reed JC, Bahr M, Weishaupt JH. Neuron-specific overexpression of the co-chaperone Bcl-2-associated athanogene-1 in superoxide dismutase 1(G93A)-transgenic mice. Neuroscience 2008; 157:844-9. doi:10.1016/j.neuroscience.2008.09.055

111. Gamerdinger M, Hajieva P, Kaya AM, Wolfrum U, Hartl FU, Behl C. Protein quality control during aging involves recruitment of the macroautophagy pathway by BAG3. EMBO J 2009; 28:889-901. doi:10.1038/emboj.2009.29
112. Demand J, Alberti S, Patterson C, Hohfeld J. Cooperation of a ubiquitin domain protein and an E3 ubiquitin ligase during chaperone/proteasome coupling. Curr Biol 2001; 11:1569-77. doi:10.1016/S0960-9822(01)00487-0
113. Alberti S, Demand J, Esser C, Emmerich N, Schild H, Hohfeld J. Ubiquitylation of BAG-1 suggests a novel regulatory mechanism during the sorting of chaperone substrates to the proteasome. J Biol Chem 2002; 277:45920-7. doi:10.1074/jbc.M204196200
114. Bejarano E, Cuervo AM. Chaperone-mediated autophagy. Proc Am Thorac Soc 2010; 7:29-39. doi:10.1513/pats.200909-102JS
115. Takayama S, Ostuni E, LeDuc P, Naruse K, Ingber DE, Whitesides GM. Subcellular positioning of small molecules. Nature 2001; 411:1016. doi:10.1038/35082637
116. Tsukahara F, Maru Y. Bag1 directly routes immature BCR-ABL for proteasomal degradation. Blood 2010; 116:3582-92. doi:10.1182/blood-2009-10-249623
117. Sroka K, Voigt A, Deeg S, Reed JC, Schulz JB, Bahr M, Kermer P. BAG1 modulates huntingtin toxicity, aggregation, degradation, and subcellular distribution. J Neurochem 2009; 111:801-7. doi:10.1111/j.1471-4159.2009.06363.x
118. Johnston JA, Ward CL, Kopito RR. Aggresomes: a cellular response to misfolded proteins. J Cell Biol 1998; 143:1883-98. doi:10.1083/jcb.143.7.1883
119. Lamark T, Johansen T. Aggrephagy: selective disposal of protein aggregates by macroautophagy. Int J Cell Biol 2012; 2012:736905. doi:10.1155/2012/736905
120. Webb JL, Ravikumar B, Rubinsztein DC. Microtubule disruption inhibits autophagosome-lysosome fusion: implications for studying the roles of aggresomes in polyglutamine diseases. Int J Biochem Cell Biol 2004; 36:2541-50. doi:10.1016/j.biocel.2004.02.003
121. Kopito RR. Aggresomes, inclusion bodies and protein aggregation. Trends Cell Biol 2000; 10:524-30. doi:10.1016/S0962-8924(00)01852-3
122. Kopito RR, Ron D. Conformational disease. Nat Cell Biol 2000; 2:E207-9. doi: 10.1038/35041139
123. Kettern N, Rogon C, Limmer A, Schild H, Hohfeld J. The Hsc/Hsp70 co-chaperone network controls antigen aggregation and presentation during maturation of professional antigen presenting cells. PLoS One 2011; 6:e16398. doi:10.1371/journal.pone.0016398
124. Puls I, Jonnakuty C, LaMonte BH, Mann E, Floeter MK, Bidus K, Drayna D, Oh SJ, Brown Jr RH, Ludlow CL, et al. Mutant dynactin in motor neuron disease. Nat Genet 2003; 33:455 - 6. doi:10.1038/ng1123
125. Levy JR, Sumner CJ, Caviston JP, Tokito MK, Ranganathan S, Ligon LA, Wallace KE, LaMonte BH, Harmison GG, Puls I, et al. A motor neuron disease-associated mutation in p150Glued perturbs dynactin function and induces protein aggregation. J Cell Biol 2006; 172:733-45. doi:10.1083/jcb.200511068
126. Kuzma-Kozakiewicz M, Usarek E, Ludolph AC, Baranczyk-Kuzma A. Mice with mutation in dynein heavy chain 1 do not share the same tau expression pattern with mice with SOD1-related motor neuron disease. Neurochem Res 2011; 36:978-85. doi:10.1007/s11064-011-0436-z
127. Schiavo G, Greensmith L, Hafezparast M, Fisher EM. Cytoplasmic dynein heavy chain: the servant of many masters. Trends Neurosci 2013; 36:641-51. doi:10.1016/j.tins.2013.08.001
128. Kieran D, Hafezparast M, Bohnert S, Dick JR, Martin J, Schiavo G, Fisher EM, Greensmith L. A mutation in dynein rescues axonal transport defects and extends the life span of ALS mice. J Cell Biol 2005; 169:561-7. doi: 10.1083/jcb.200501085
129. Teuling E, van Dis V, Wulf PS, Haasdijk ED, Akhmanova A, Hoogenraad CC, Jaarsma D. A novel mouse model with impaired dynein/dynactin function develops amyotrophic lateral

sclerosis (ALS)-like features in motor neurons and improves lifespan in SOD1-ALS mice. Hum Mol Genet 2008; 17:2849-62. doi: 10.1093/hmg/ddn182
130. Nollen EA, Brunsting JF, Song J, Kampinga HH, Morimoto RI. Bag1 functions in vivo as a negative regulator of Hsp70 chaperone activity. Mol Cell Biol 2000; 20:1083-8. doi:10.1128/MCB.20.3.1083-1088.2000
131. Tortarolo M, Crossthwaite AJ, Conforti L, Spencer JP, Williams RJ, Bendotti C, Rattray M. Expression of SOD1 G93A or wild-type SOD1 in primary cultures of astrocytes down-regulates the glutamate transporter GLT-1: lack of involvement of oxidative stress. J Neurochem 2004; 88:481-93. doi:10.1046/j.1471-4159.2003.02208.x
132. Ayala YM, Misteli T, Baralle FE. TDP-43 regulates retinoblastoma protein phosphorylation through the repression of cyclin-dependent kinase 6 expression. Proc Natl Acad Sci U S A 2008; 105:3785-9. doi:10.1073/pnas.0800546105
133. Ayala YM, Zago P, D'Ambrogio A, Xu YF, Petrucelli L, Buratti E, Baralle FE. Structural determinants of the cellular localization and shuttling of TDP-43. J Cell Sci 2008; 121:3778-85. doi:10.1073/pnas.0800546105
134. Cashman NR, Durham HD, Blusztajn JK, Oda K, Tabira T, Shaw IT, Dahrouge S, Antel JP. Neuroblastoma x spinal cord (NSC) hybrid cell lines resemble developing motor neurons. Dev Dyn 1992; 194:209-21. doi:10.1002/aja.1001940306
135. Durham HD, Dahrouge S, Cashman NR. Evaluation of the spinal cord neuron X neuroblastoma hybrid cell line NSC-34 as a model for neurotoxicity testing. Neurotoxicol 1992; 14:387-95.
136. Marron TU, Guerini V, Rusmini P, Sau D, Brevini TAL, Martini L, Poletti A. Androgen-induced neurite outgrowth is mediated by neuritin in motor neurones. J Neurochem 2005; 92:10-20. doi:10.1111/j.1471-4159.2004.02836.x
137. Locatelli D, Terao M, Fratelli M, Zanetti A, Kurosaki M, Lupi M, Barzago MM, Uggetti A, Capra S, D'Errico P, et al. Human axonal survival of motor neuron (a-SMN) protein stimulates axon growth, cell motility, C-C motif ligand 2 (CCL2), and insulin-like growth factor-1 (IGF1) production. J Biol Chem 2012; 287:25782-94. doi:10.1074/jbc.M112.362830
138. Ferri A, Cozzolino M, Crosio C, Nencini M, Casciati A, Gralla EB, Rotilio G, Valentine JS, Carri MT. Familial ALS-superoxide dismutases associate with mitochondria and shift their redox potentials. Proc Natl Acad Sci U S A 2006; 103:13860-5. doi:10.1073/pnas.0605814103
139. Poletti A, Rampoldi A, Piccioni F, Volpi S, Simeoni S, Zanisi M, Martini L. 5Alpha-reductase type 2 and androgen receptor expression in gonadotropin releasing hormone GT1-1 cells. J Neuroendocrinol 2001; 13:353-7. doi:10.1046/j.1365-2826.2001.00635.x
140. Pozzi P, Bendotti C, Simeoni S, Piccioni F, Guerini V, Marron TU, Martini L, Poletti A. Androgen 5-alpha-reductase type 2 is highly expressed and active in rat spinal cord motor neurones. J Neuroendocrinol 2003; 15:882-7. doi:10.1046/j.1365-2826.2003.01074.x
141. Rusmini P, Polanco MJ, Cristofani R, Cicardi ME, Meroni M, Galbiati M, Piccolella M, Messi E, Giorgetti E, Lieberman AP, et al. Aberrant Autophagic Response in The Muscle of A Knock-in Mouse Model of Spinal and Bulbar Muscular Atrophy. Sci Rep 2015; 5:15174. doi:10.1038/srep15174.
142. Crippa V, Boncoraglio A, Galbiati M, Aggarwal T, Rusmini P, Giorgetti E, Cristofani R, Carra S, Pennuto M, Poletti A. Differential autophagy power in the spinal cord and muscle of transgenic ALS mice. Front Cell Neurosci 2013; 7:234. doi:10.3389/fncel.2013.00234
143. Koyama S, Arawaka S, Chang-Hong R, Wada M, Kawanami T, Kurita K, Kato M, Nagai M, Aoki M, Itoyama Y, et al. Alteration of familial ALS-linked mutant SOD1 solubility with disease progression: its modulation by the proteasome and Hsp70. Biochem Biophys Res Commun 2006; 343:719-30. doi:10.1016/j.bbrc.2006.02.170
144. Allen S, Heath PR, Kirby J, Wharton SB, Cookson MR, Menzies FM, Banks RE, Shaw PJ. Analysis of the cytosolic proteome in a cell culture model of familial amyotrophic lateral

sclerosis reveals alterations to the proteasome, antioxidant defenses, and nitric oxide synthetic pathways. J Biol Chem 2003; 278:6371-83. doi:10.1074/jbc.M209915200

Legends to figures

Figure 1. Autophagic clearance of ARpolyQ. NSC34 cells cotransfected with AR.Q46 and pCDNA3 or HSPB8, and treated with vehicle (ethanol, EtOH) or 10 nM T, for 48 h. (**A**) Immunofluorescence microscopy (IF) analysis (63x magnification) of AR (green); nuclei were stained with DAPI (blue); scale bar: 20 μm. (**B**) WB and FRA show AR.Q46 total levels and AR.Q46 insoluble fraction respectively. TUBA was used as loading control. Bar graph represents the FRA mean relative optical density computed over 3 independent biological samples for each condition (n=3) ± SD (*=P<0.05, ***=P<0.001; Two-Way ANOVA followed by the Uncorrected Fisher LSD test). (**C**) Phase contrast imaging and IF performed on NSC34 cells transfected with *Dync1h1* siRNA show cell morphology and dynein distribution. Scale bar: 20 μm. (**D**) WB analysis of NSC34 cells transfected with *Dync1h1* siRNA shows the levels of dynein heavy chain; TUBA was used as loading control. Bar graph represents the WB mean relative optical density measured over 3 independent biological samples for each condition (n=3) ± SD (**=P<0.01, one-tailed unpaired Student t test). (**E**) FRA and WB of NSC34 stably expressing GFP-AR.Q39 and transfected with *Dync1h1* siRNA show AR.Q39 insoluble fraction accumulation after 10 nM T treatment and reduction after dynein silencing. Bar graph represents the FRA mean relative optical density computed over 3 independent biological samples for each condition (n=3) ± SD (*=P<0.05, **=P<0.01; Two-Way ANOVA followed by the Uncorrected Fisher LSD test).

Figure 2. Effect of dynein-silencing on autophagy and ARpolyQ clearance. (**A**) Confocal microscopy analysis (40x magnification) performed on NSC34 cells transfected with *Dync1h1* siRNA shows SQSTM1 or LC3 distribution (green); nuclei were stained with DAPI (blue); scale bars: 50 μm. Bar graphs represent the quantification of total green-fluorescence integrated density (IntDen) normalized on cells number. Six images were analyzed for each condition. (**B**) WB of LC3-I and LC3-II levels performed on NSC34 transfected with *Dync1h1* siRNA and treated with 20

mM NH_4Cl for the last 1.5 h. Nontargeting siRNA was used as control; TUBA was used as loading control. Bar graph represents the mean relative optical density computed over 3 independent biological samples for each condition (n=3) ± SD (*=*P*<0.05, **=*P*<0.01; Two-Way ANOVA followed by the Uncorrected Fisher LSD test); (**C**) WB of LC3-I and LC3-II levels performed on NSC34 treated with 100 μM EHNA and/or 20 mM NH_4Cl for the last 1.5 h. Nontargeting siRNA was used as control; TUBA was used as loading control. Bar graphs represent the mean relative optical density computed over 3 independent biological samples for each condition (n=3) ± SD (*=*P*<0.05, **=*P*<0.01; Two-Way ANOVA followed by the Uncorrected Fisher LSD test).

Figure 3. Autophagy modulation by EHNA treatment. NSC34 cells treated with DMSO, 100 μM EHNA and/or 100 mM trehalose for 48 h; (**A**, **B**) the bar graph represents *Sqstm1* and *Lc3* mRNA relative levels normalized with *Rplp0* mRNA levels. Analysis was conducted on 4 independent biological samples for each condition (n=4) ± SD (**=*P*<0.01, ***=*P*<0.001; Two-Way ANOVA followed by the Uncorrected Fisher LSD test). (**C**) Confocal microscopy analysis shows SQSTM1 and LC3 localization (40x magnification); scale bars: 50 μm. Bar graph represents the quantification of total green fluorescence integrated density (IntDen) normalized on cells number. Six images were analyzed for each condition (n=6) ± SD (**=*P*<0.01, **=*P*<0.001; one-tailed unpaired Student t test). Lower gain was used to acquire trehalose-treated cells (low sensitivity [L.S.]) compared to control (high sensitivity [H.S.]). (**D**) WB analysis shows SQSTM1 and LC3 levels; TUBA was used as loading control. Bar graphs represent the mean relative optical density computed over 3 independent biological samples for each condition (n=3) ± SD of SQSTM1:TUBA (middle inset) and LC3-II:TUBA (low inset) ratio (*=*P*<0.05, **=*P*<0.01, ***=*P*<0.001; One-Way ANOVA followed by the Uncorrected Fisher LSD test).

Figure 4. Effect of dynein ATPase activity-inhibition on ARpolyQ clearance. FRA and WB show ARpolyQ total levels and ARpolyQ insoluble fraction, respectively, of: (**A**) PC12 cells stably

transfected with AR.Q10 and AR.Q112 induced with 1 μg/mL doxycycline for 72 h. Cells were treated with ethanol (EtOH) or 10 nM T and/or EHNA 100 μM for the last 48 h prior to analysis. TUBA was used as loading control and bar graphs represent the FRA mean relative optical density computed over 3 independent biological samples for each condition (n=3) ± SD (***=P<0.001; One-Way ANOVA followed by the Uncorrected Fisher LSD test); (**B**) TR4 NSC34 cells stably transfected with GFP-AR.Q0 induced with 1 μg/mL doxycycline for 72 h; (**C**) TR4 NSC34 cells stably transfected with GFP-AR.Q39 induced with 1 μg/mL doxycycline for 72 h; (**D**) NSC34 cells transiently transfected with AR.Q46 for 48 h. Cells were treated with ethanol (EtOH) or 10 nM T and/or EHNA 100 μM for the last 48 h prior to analysis. (**C** and **D**) TUBA was used as loading control and bar graphs represent the FRA mean relative optical density computed over 3 independent biological samples for each condition (n=3) ± SD (*=P<0.05, **=P<0.01; Two-Way ANOVA followed by the Uncorrected Fisher LSD test). (**E**) IF performed on NSC34 cells transfected with AR.Q46 and treated with 10 nM T or EtOH and 100 μM EHNA or DMSO for 48 h. AR was stained with AR H280 antibody (green), nuclei were stained with DAPI (blue) (63x magnification); scale bar: 20 μm. (**F**) Bar graph represents the mean percentage of transfected cells with inclusions computed over 3 independent biological samples for each condition (n=3) ± SD (*=P<0.05, ***=P<0.001; Two-Way ANOVA followed by the Uncorrected Fisher LSD test). Ten fields for each biological sample were analyzed. (**G**) WB analysis of PBS, Triton X100, SDS and FA lysates fractions of NSC34 cells transfected with AR.Q46 and treated with 10 nM T or EtOH and 100 μM EHNA or DMSO for 48 h. GAPDH was used as loading control.

Figure 5. Dynein ATPase activity inhibition promotes ARpolyQ clearance via UPS. (**A**) NSC34 cells stably transfected with GFP-AR.Q39, treated with 10 nM T, 10 mM 3MA and/or 100 μM EHNA for the last 48 h and/or 10 μM MG132 for the last 16 h. WB shows ARpolyQ levels and FRA shows ARpolyQ insoluble fraction. Bar graph represents the FRA mean relative optical

density computed over 3 independent biological samples for each condition (n=3) ± SD (**=*P*<0.01; ***=*P*<0.001; one-tailed unpaired Student t test). (**B**) NSC34 cells transfected with GFPu reporter and/or ARpolyQ and treated with 10 nM T and/or 100 μM EHNA. WB shows ARpolyQ and GFPu bands; TUBA was used as loading control. Bar graph represents the GFP WB densitometric analysis of 3 independent samples for each condition (n=3) ± SD (*=*P*<0.05; ***=*P*<0.001; Two-Way ANOVA followed by the Uncorrected Fisher LSD test); (**C**) Proteasome chymotryptic activity assay performed on NSC34 treated with DMSO or 100 μM EHNA and 10 μM MG132 used as negative control. Bar graph represents the mean relative fluorescence normalized on control group and computed over 4 independent biological samples for each condition (n=4) ± SD (***=*P*<0.001, One-Way ANOVA followed by the Uncorrected Fisher LSD test). (**D**) Proteasome chymotryptic activity assay performed on NSC34 transfected with AR.Q46 and treated with 10 nM T, DMSO or 100 μM EHNA and 10 μM MG132 used as negative control. Bar graph represents the mean relative fluorescence normalized on control group and computed over 4 independent biological samples for each condition (n=4) ± SD (***=*P*<0.001, One-Way ANOVA followed by the Uncorrected Fisher LSD test). (**E**) β-galactosidase assay performed on NSC34 cells transfected with pCMV-β and treated with DMSO or 100 μM EHNA for 24 or 48 h after transfection. Bar graph represents the mean relative absorbance normalized on transfected cells treated for 48 h and computed over 6 independent biological samples for each condition (n=6) ± SD (Two-Way ANOVA, not significant). (**F**) MTT assay performed on NSC34 cells treated with DMSO or 100 μM EHNA for 24 or 48 h. Bar graph represents the mean relative absorbance normalized on untreated group and computed over 6 independent biological samples for each condition (n=6) ± SD (One-Way ANOVA, not significant).

Figure 6. BAG1 upregulation reduces ARpolyQ accumulation. (**A** to **C**) NSC34 cells treated with DMSO or 100 μM EHNA for 48 h. The bar graphs represent *Hspb8* (**A**), *Bag3* (B) and *Bag1* (**C**)

mRNA levels normalized with *Rplp0* mRNA levels. Four independent biological samples for each condition were analyzed (n=4) ± SD (***=*P*<0.001; One-Way ANOVA followed by the Uncorrected Fisher LSD test). (**D**) NSC34 cells overexpressing AR.Q46 alone or coexpressing BAG1 and treated with T for last 48 h. FRA shows insoluble AR-polyQ levels (upper panel) and bar graph represents the FRA mean relative optical density computed over 3 independent biological samples for each condition (n=3) ± SD (*=*P*<0.05, ***=*P*<0.001; Two-Way ANOVA followed by the Uncorrected Fisher LSD test). WB (lower panel) shows AR.Q46 and BAG1 protein levels. (**E**) NSC34 cells expressing AR.Q46 alone or coexpressing BAG1 and treated with 10 nM T for last 48 h and/or 10 μM MG132 for last 16 h. FRA shows insoluble AR-polyQ levels, bar graph represents the FRA mean relative optical density computed over 3 independent biological samples for each condition (n=3) ± SD (*=*P*<0.05, ***=*P*<0.001; Two-Way ANOVA followed by the Uncorrected Fisher LSD test and one-tailed unpaired Student t test for control condition). (**F**) WB analysis of NSC34 cells transfected with *Bag1* siRNA shows the levels of BAG1; TUBA was used as loading control. Bar graph represents the WB mean relative optical density computed over 3 independent biological samples for each condition (n=3) ± SD (**=*P*<0.01, one-tailed unpaired Student t test). (**G**) FRA and WB of NSC34 transfected with AR.Q46 and with *Bag1* siRNA shows AR.Q46 insoluble fraction; TUBA was used as loading control. Bar graph represents the FRA densitometric analysis of 3 independent biological samples for each condition (n=3) ± SD (**=*P*<0.01; ***=*P*<0.001; one-tailed unpaired Student t test).

Figure 7. EHNA effects on neuronal and motoneuronal cells obtained by differentiation of human iPSCs generated from SBMA patients. (**A**) IF analysis of neuronal and motoneuronal cells obtained by differentiation of human iPSCs generated from SBMA patients and treated with ethanol or 10 nM T (40x magnification). TUBB3 (green) and SMI312 (red) (upper inset), AR (green) and MNX1/HB9 (red) (lower inset). Nuclei were stained with DAPI (blue); scale bars: 30 μm. (**B**) Bar graph represents the percentage of MNX1/HB9-positive cells; 6 fields for each condition were

analyzed (n=6) ± SD (one-tailed unpaired Student t test, not significant). (**C** to **I**) RealTime PCR analyses performed on iPSCs differentiated to neuronal cells treated with 10 nM T and/or 100 μM EHNA for last 48 h. The bar graphs represent *HSPB8* (**C**), *BAG3* (**D**), *BAG1* (**E**), *SQSTM1* (**F**), *LC3* (**G**), *TFEB* (**H**) and *BECN1* (**I**) mRNA levels normalized with *RPLP0* mRNA levels. Four independent samples for each condition were analyzed (n=4) ± SD (*=*P*<0.05, **=*P*<0.01, ***=*P*<0.001; Two-Way ANOVA followed by the Uncorrected Fisher LSD test).

Figure 8. Effects of dynein inhibition on SOD1 and TARDBP insoluble species. (**A**) NSC34 cells expressing wtSOD1 and $SOD1^{G93A}$ treated with DMSO or 100 μM EHNA for last 48 h. FRA shows $SOD1^{G93A}$ accumulation compared to wtSOD1 and $SOD1^{G93A}$ reduction after 100 μM EHNA treatment. WB shows total level of transfected SOD1, TUBA was used as loading control. (**B**) NSC34 stably transfected with wtSOD1 or $SOD1^{G93A}$ induced with doxycycline and treated with DMSO or 100 μM EHNA for last 48 h. FRA shows $SOD1^{G93A}$ accumulation compared to wtSOD1 and $SOD1^{G93A}$ reduction after 100 μM EHNA treatment. WB shows total level of transfected SOD1, TUBA was used as loading control. (**C**) NSC34 expressing FL and $TARDBP^{\Delta C}$ treated with DMSO or 100 μM EHNA for last 48 h. FRA shows $TARDBP^{\Delta C}$ accumulation compared to FL TARDBP and $TARDBP^{\Delta C}$ reduction after 100 μM EHNA treatment. WB shows total level of transfected TARDBP, TUBA was used as loading control; (**A to C**) Bar graphs represent the FRA mean relative optical density computed over 3 independent biological samples for each condition (n=3) ± SD (**=*P*<0.01, ***=*P*<0.001; Two-Way ANOVA followed by the Uncorrected Fisher LSD test). (**D** and **E**) NSC34 expressing $SOD1^{G93A}$ (**D**) or $TARDBP^{\Delta C}$ (**E**) and treated with DMSO, 100 μM EHNA and/or 10 mM 3MA for the last 48 h and 10 μM MG132 for the last 16 h. FRAs show $SOD1^{G93A}$ (**D**) or $TARDBP^{\Delta C}$ (**E**) accumulation after 3MA and MG132 treatments. EHNA treatment counteracts 3MA activity but not MG132 activity. WBs show total level of transfected SOD1 (**D**) or $TARDBP^{\Delta C}$ (**E**), TUBA or GAPDH was used as loading control. Bar graphs represent

the FRA mean relative optical density computed over 3 independent biological samples for each condition (n=3) ± SD (*=*P*<0.05, **=*P*<0.01, ***=*P*<0.001; Two-Way ANOVA followed by the Uncorrected Fisher LSD test and one-tailed unpaired Student t test for control conditions).

Figure 9. Effects of dynein inhibition on poly-GP insoluble fraction. (**A**) NSC34 cells expressing poly-GP (100 repeats) treated with 10 mM 3MA and/or 100 μM EHNA for the last 48 h prior to analysis and/or 10 μM MG132 for the last 16 h prior to analysis. FRA shows poly-GP insoluble fraction. Bar graphs represent the FRA mean relative optical density computed over 3 independent biological samples for each condition (n=3) ± SD (**=*P*<0.01; ***=*P*<0.001; one-tailed unpaired Student t test); (**B**) the portion shown in A by the rectangle has been magnified to show the differences between short bars. WB shows total level of transfected poly-GP; TUBA was used as loading control.

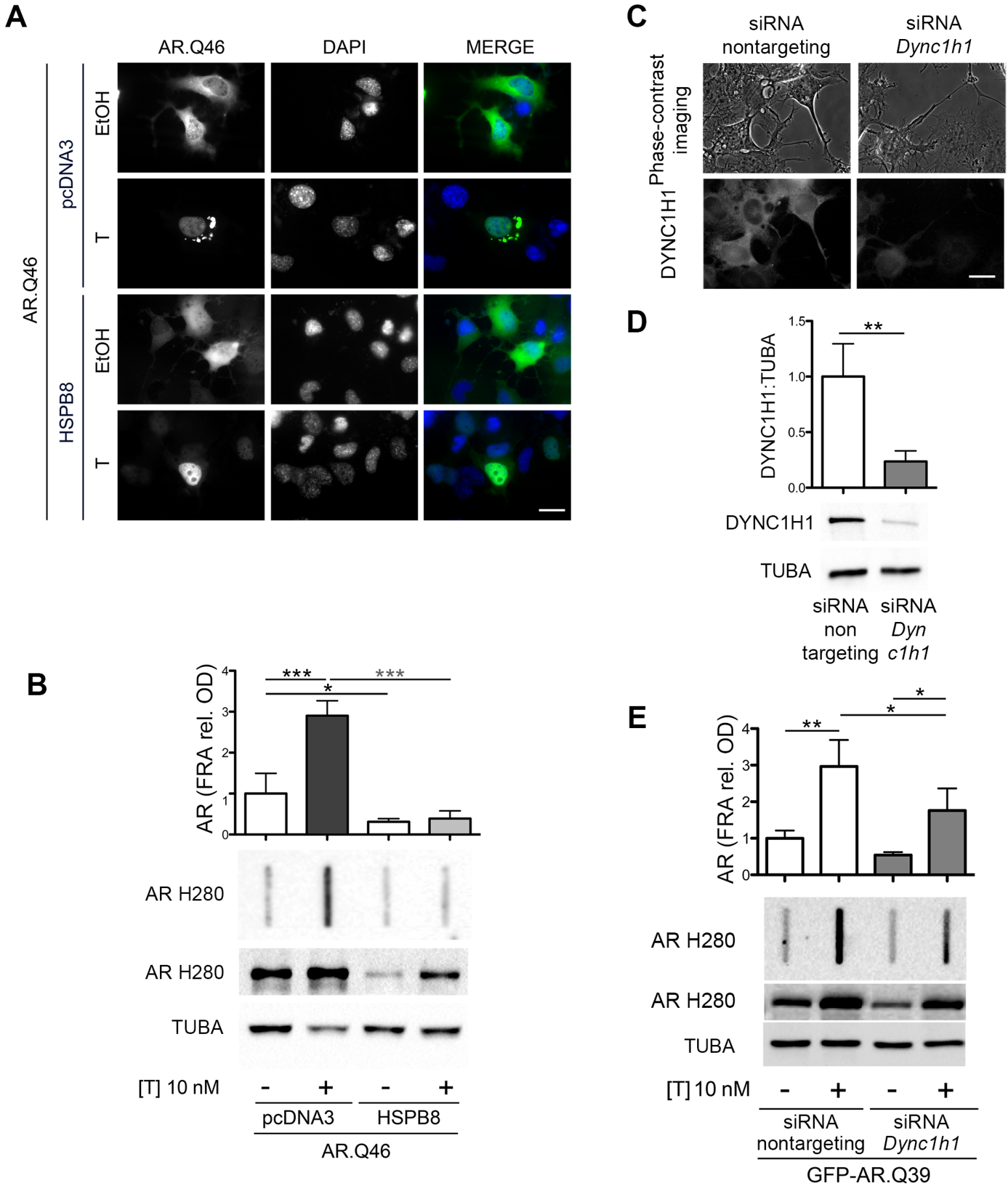
A
AR.Q46
DAPI
MERGE
AR.Q46
pcDNA3
HSPB8
EtOH
T
EtOH
T
C
siRNA nontargeting
siRNA Dync1h1
Phase-contrast imaging
DYNC1H1
D
DYNC1H1:TUBA
1.5
1.0
0.5
0.0
**
DYNC1H1
TUBA
siRNA non targeting
siRNA Dync1h1
B
AR (FRA rel. OD)
***
***
*
AR H280
AR H280
TUBA
[T] 10 nM
- + - +
pcDNA3
HSPB8
AR.Q46
E
AR (FRA rel. OD)
**
*
*
AR H280
AR H280
TUBA
[T] 10 nM
- + - +
siRNA nontargeting
siRNA Dync1h1
GFP-AR.Q39

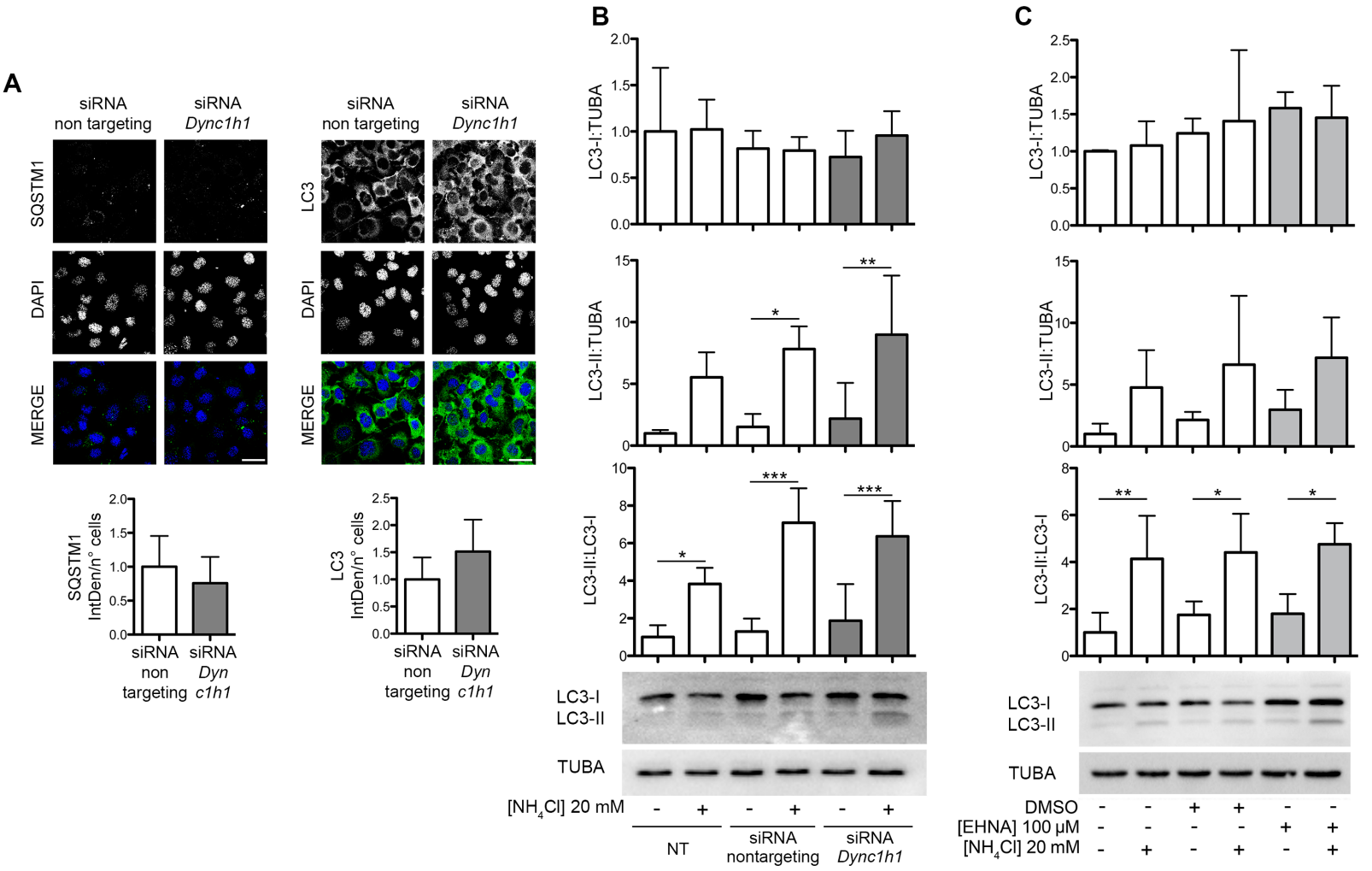
A
siRNA non targeting
siRNA Dync1h1
SQSTM1
DAPI
MERGE
LC3
SQSTM1 IntDen/n° cells
LC3 IntDen/n° cells
siRNA non targeting
siRNA Dync1h1
B
LC3-I:TUBA
LC3-II:TUBA
LC3-II:LC3-I
LC3-I
LC3-II
TUBA
[NH4Cl] 20 mM
NT
siRNA nontargeting
siRNA Dync1h1
C
DMSO
[EHNA] 100 µM
[NH4Cl] 20 mM

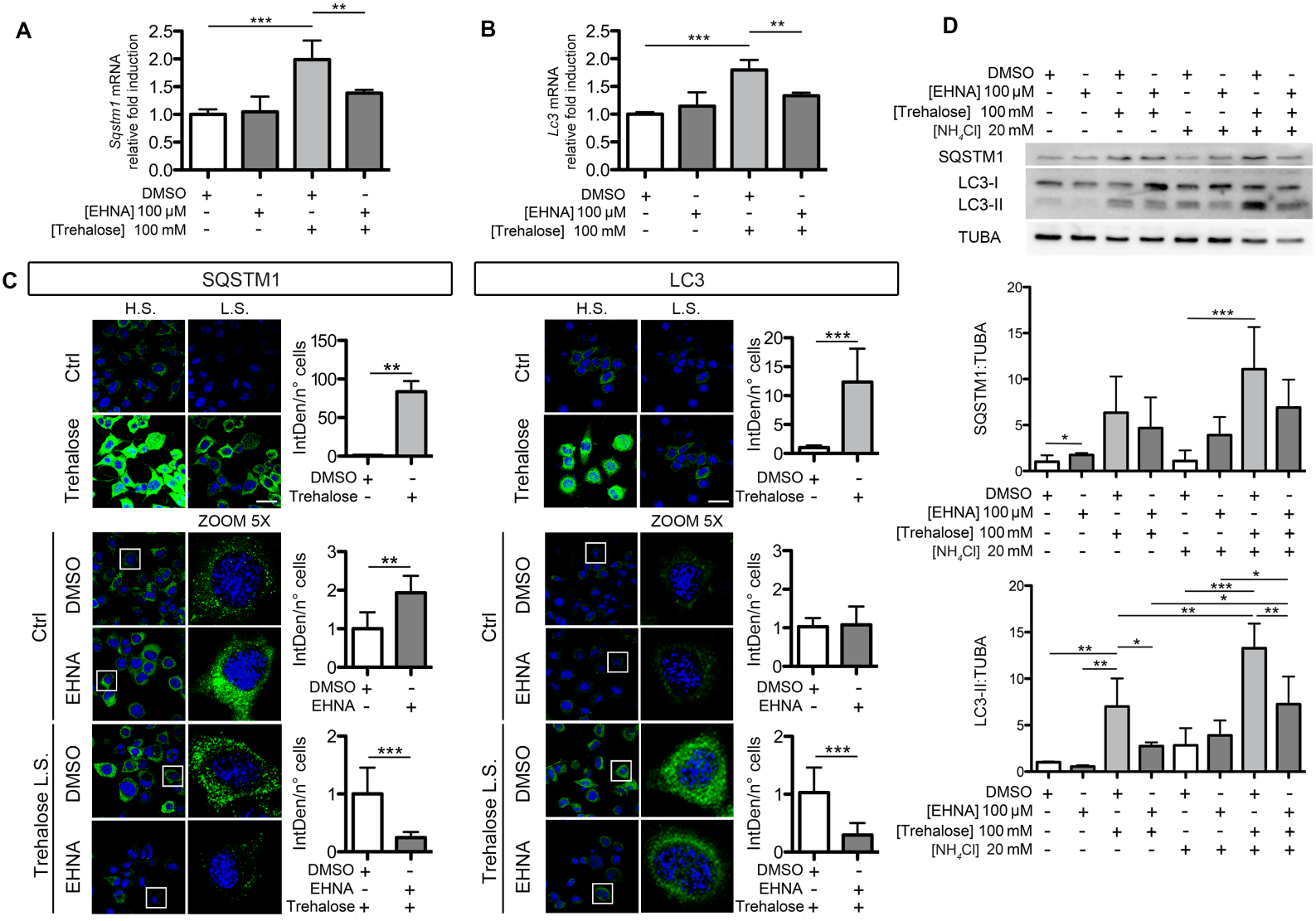
A
Sqstm1 mRNA relative fold induction
2.5
2.0
1.5
1.0
0.5
0.0
***
**
DMSO + - + -
[EHNA] 100 µM - + - +
[Trehalose] 100 mM - - + +
B
Lc3 mRNA relative fold induction
2.5
2.0
1.5
1.0
0.5
0.0
***
**
DMSO + - + -
[EHNA] 100 µM - + - +
[Trehalose] 100 mM - - + +
D
DMSO + - + - + - + -
[EHNA] 100 µM - + - + - + - +
[Trehalose] 100 mM - - + + - - + +
[NH4Cl] 20 mM - - - - + + + +
SQSTM1
LC3-I
LC3-II
TUBA
C
SQSTM1
LC3
H.S.
L.S.
Ctrl
Trehalose
IntDen/n° cells
150
100
50
0
**
DMSO + -
Trehalose - +
20
15
10
5
0
***
DMSO + -
Trehalose - +
ZOOM 5X
Ctrl
DMSO
EHNA
3
2
1
0
**
DMSO + -
EHNA - +
***
DMSO + -
EHNA - +
Trehalose + +
Trehalose L.S.
DMSO
EHNA
SQSTM1:TUBA
20
15
10
5
0
*
***
DMSO + - + - + - + -
[EHNA] 100 µM - + - + - + - +
[Trehalose] 100 mM - - + + - - + +
[NH4Cl] 20 mM - - - - + + + +
LC3-II:TUBA
20
15
10
5
0
**
**
*
***
*
**
**
*
DMSO + - + - + - + -
[EHNA] 100 µM - + - + - + - +
[Trehalose] 100 mM - - + + - - + +
[NH4Cl] 20 mM - - - - + + + +

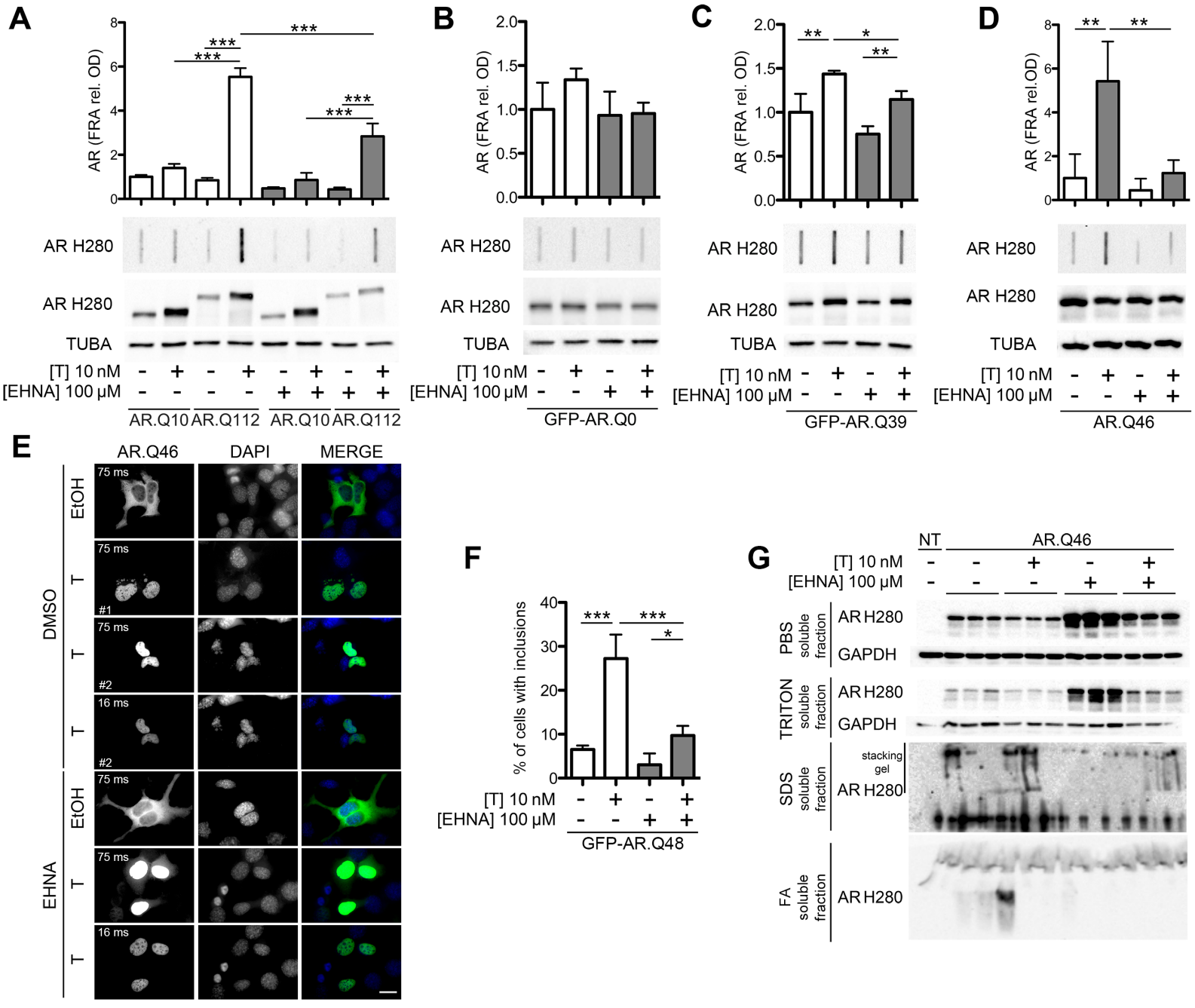
A
AR (FRA rel. OD)
AR H280
AR H280
TUBA
[T] 10 nM
[EHNA] 100 µM
AR.Q10
AR.Q112
AR.Q10
AR.Q112
B
AR (FRA rel. OD)
AR H280
AR H280
TUBA
[T] 10 nM
[EHNA] 100 µM
GFP-AR.Q0
C
AR (FRA rel. OD)
AR H280
AR H280
TUBA
[T] 10 nM
[EHNA] 100 µM
GFP-AR.Q39
D
AR (FRA rel.OD)
AR H280
AR H280
TUBA
[T] 10 nM
[EHNA] 100 µM
AR.Q46
E
AR.Q46
DAPI
MERGE
DMSO
EHNA
EtOH
T
75 ms
16 ms
#1
#2
F
% of cells with inclusions
[T] 10 nM
[EHNA] 100 µM
GFP-AR.Q48
G
NT
AR.Q46
[T] 10 nM
[EHNA] 100 µM
PBS soluble fraction
TRITON soluble fraction
SDS soluble fraction
FA soluble fraction
AR H280
GAPDH
stacking gel

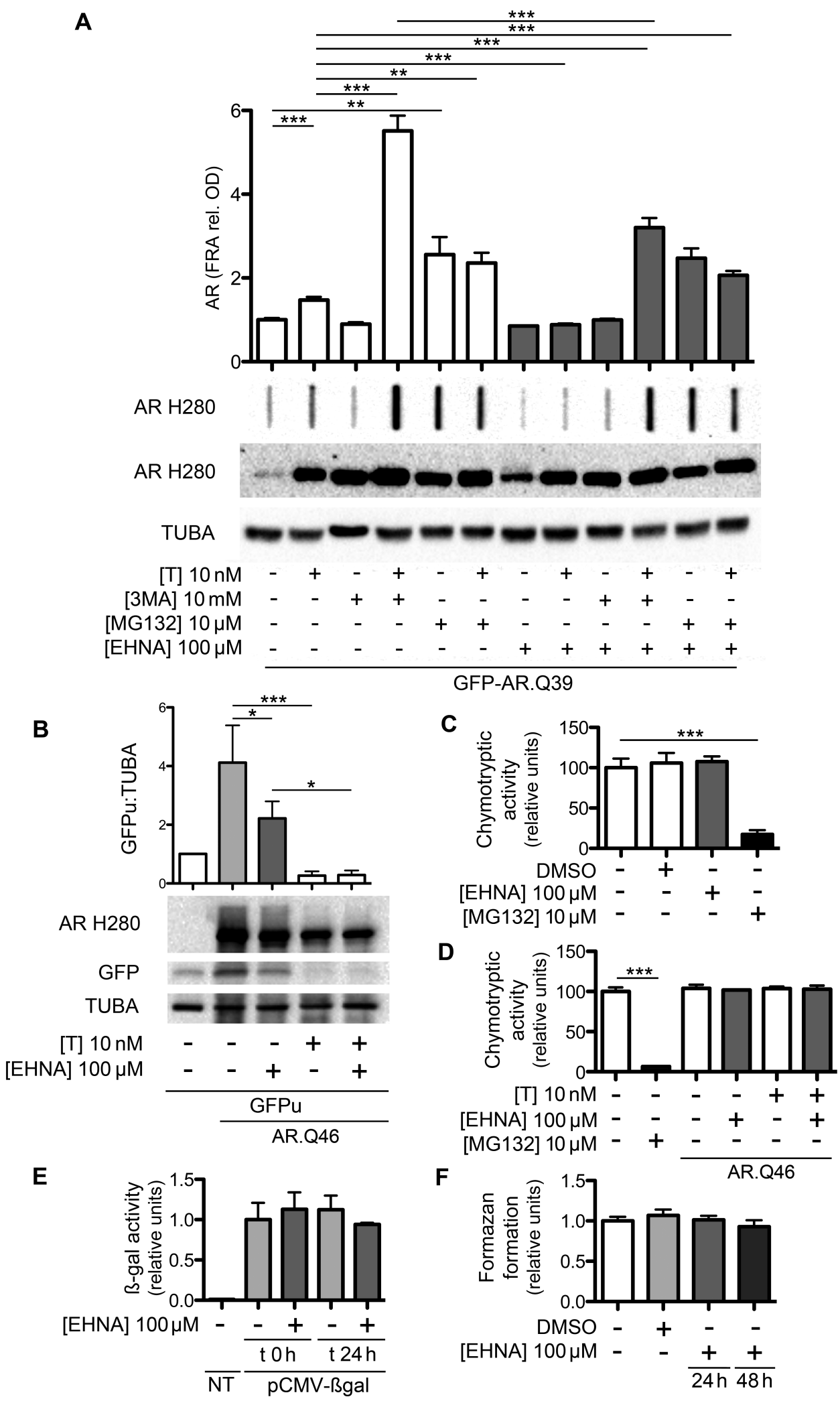
A
AR (FRA rel. OD)
AR H280
AR H280
TUBA
[T] 10 nM
[3MA] 10 mM
[MG132] 10 µM
[EHNA] 100 µM
GFP-AR.Q39
B
GFPu:TUBA
AR H280
GFP
TUBA
[T] 10 nM
[EHNA] 100 µM
GFPu
AR.Q46
C
Chymotryptic activity (relative units)
DMSO
[EHNA] 100 µM
[MG132] 10 µM
D
Chymotryptic activity (relative units)
[T] 10 nM
[EHNA] 100 µM
[MG132] 10 µM
AR.Q46
E
ß-gal activity (relative units)
[EHNA] 100 µM
t 0 h
t 24 h
NT
pCMV-ßgal
F
Formazan formation (relative units)
DMSO
[EHNA] 100 µM
24 h
48 h

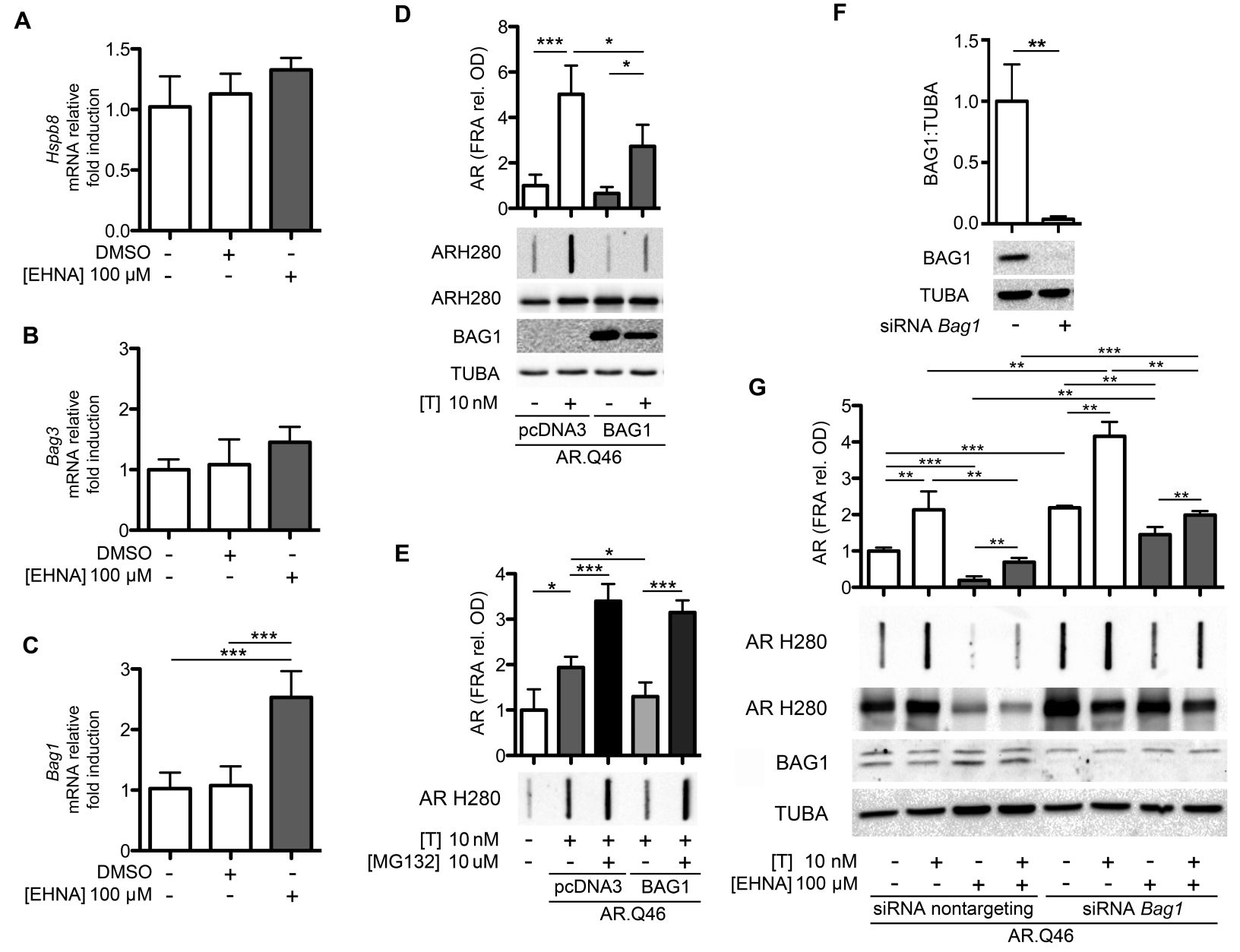
A
Hspb8 mRNA relative fold induction
1.5
1.0
0.5
0.0
DMSO - + -
[EHNA] 100 µM - - +
B
Bag3 mRNA relative fold induction
3
2
1
0
DMSO - + -
[EHNA] 100 µM - - +
C
Bag1 mRNA relative fold induction
***
***
3
2
1
0
DMSO - + -
[EHNA] 100 µM - - +
D
AR (FRA rel. OD)
***
*
*
8
6
4
2
0
ARH280
ARH280
BAG1
TUBA
[T] 10 nM - + - +
pcDNA3 BAG1
AR.Q46
E
AR (FRA rel. OD)
*
***
*
***
4
3
2
1
0
AR H280
[T] 10 nM - + + + +
[MG132] 10 uM - - + - +
pcDNA3 BAG1
AR.Q46
F
BAG1:TUBA
**
1.5
1.0
0.5
0.0
BAG1
TUBA
siRNA Bag1 - +
G
AR (FRA rel. OD)
***
**
**
**
**
***
***
**
**
**
**
5
4
3
2
1
0
AR H280
AR H280
BAG1
TUBA
[T] 10 nM - + - + - + - +
[EHNA] 100 µM - - + + - - + +
siRNA nontargeting siRNA Bag1
AR.Q46

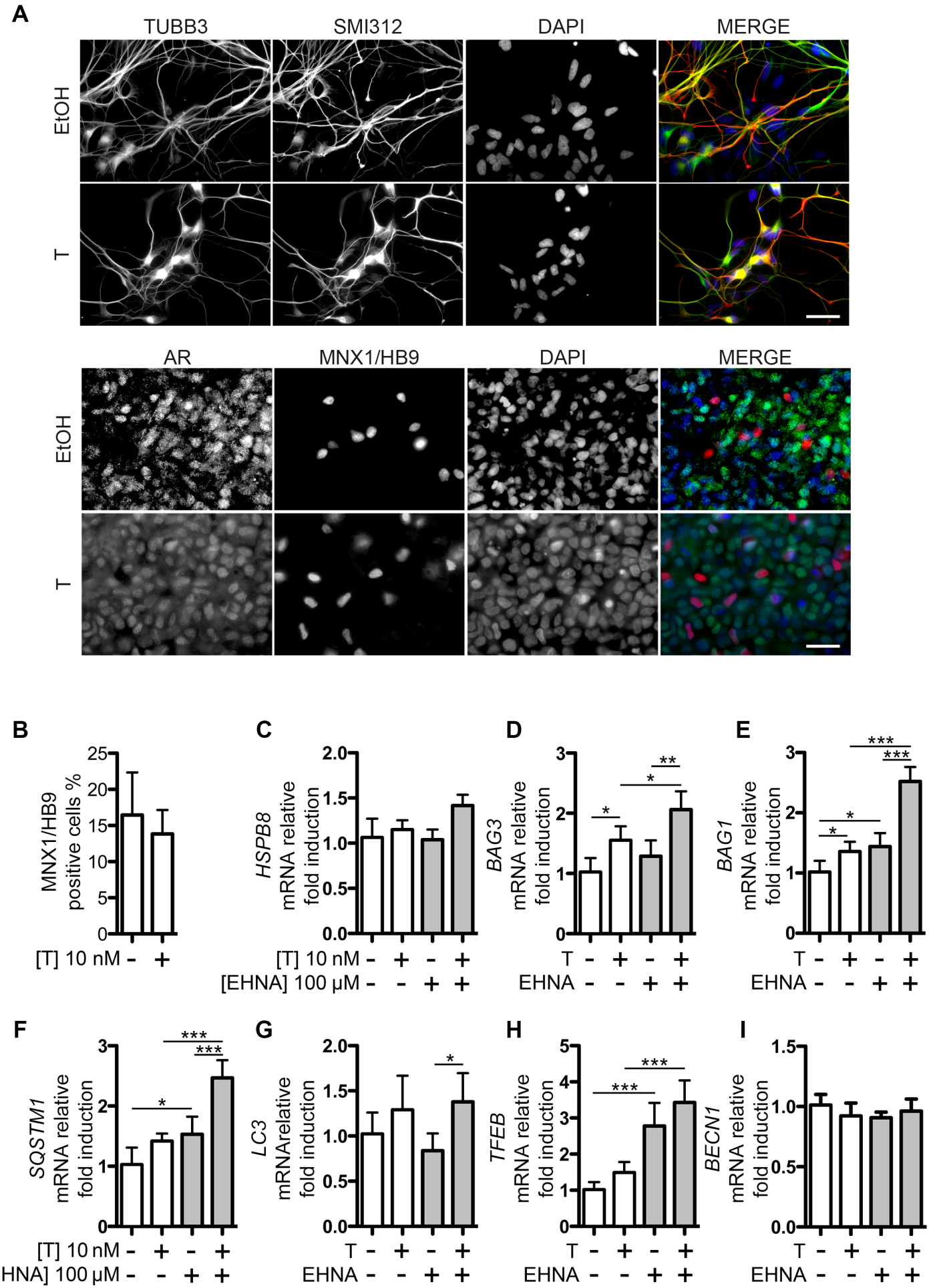
A
TUBB3
SMI312
DAPI
MERGE
EtOH
T
AR
MNX1/HB9
DAPI
MERGE
EtOH
T
B
MNX1/HB9 positive cells %
[T] 10 nM
C
HSPB8 mRNA relative fold induction
[T] 10 nM
[EHNA] 100 µM
D
BAG3 mRNA relative fold induction
T
EHNA
E
BAG1 mRNA relative fold induction
T
EHNA
F
SQSTM1 mRNA relative fold induction
[T] 10 nM
[EHNA] 100 µM
G
LC3 mRNArelative fold induction
T
EHNA
H
TFEB mRNA relative fold induction
T
EHNA
I
BECN1 mRNA relative fold induction
T
EHNA

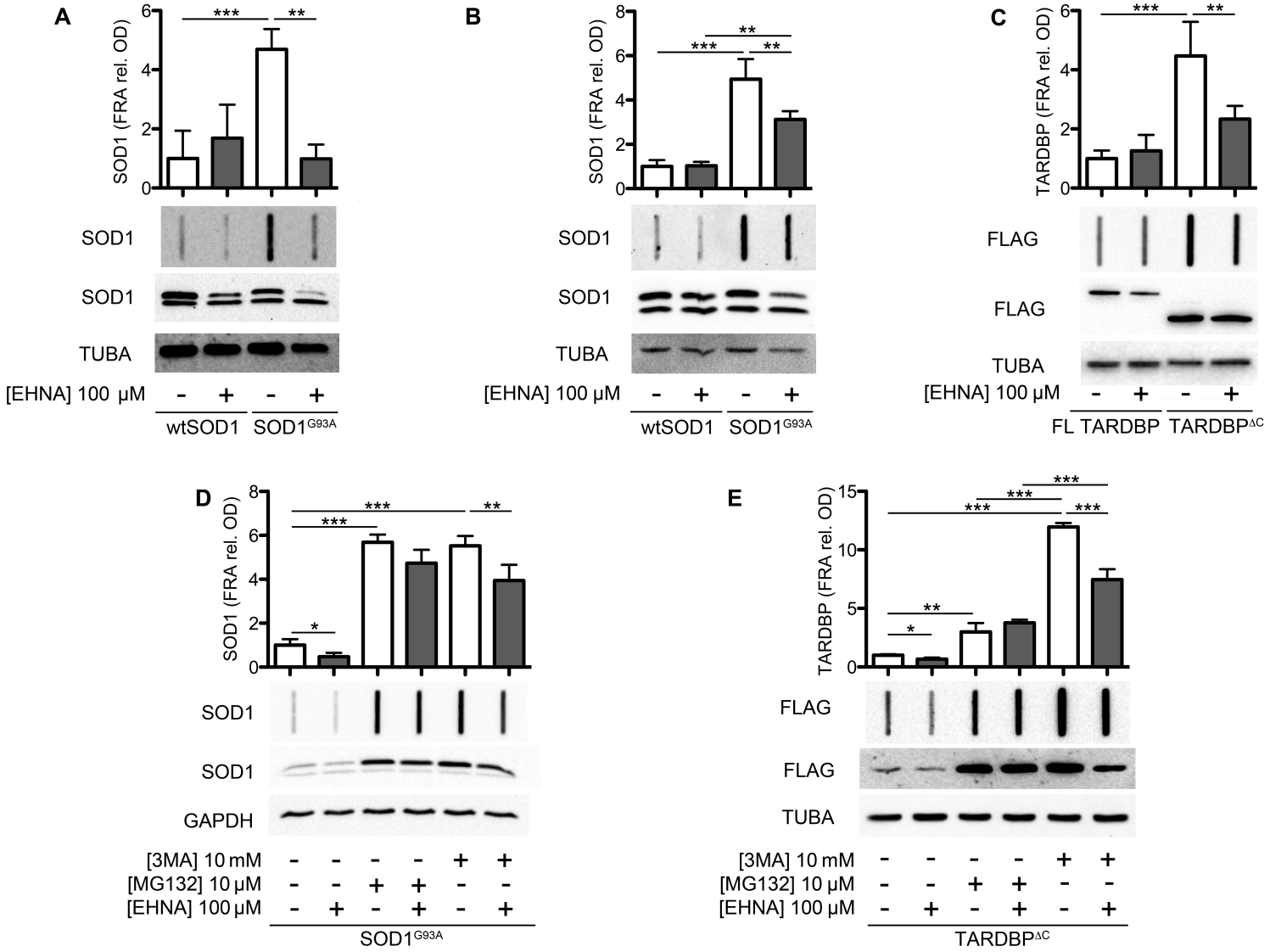
A
SOD1 (FRA rel. OD)
SOD1
SOD1
TUBA
[EHNA] 100 μM
wtSOD1
SOD1G93A
B
SOD1 (FRA rel. OD)
SOD1
SOD1
TUBA
[EHNA] 100 μM
wtSOD1
SOD1G93A
C
TARDBP (FRA rel. OD)
FLAG
FLAG
TUBA
[EHNA] 100 μM
FL TARDBP
TARDBPΔC
D
SOD1 (FRA rel. OD)
SOD1
SOD1
GAPDH
[3MA] 10 mM
[MG132] 10 μM
[EHNA] 100 μM
SOD1G93A
E
TARDBP (FRA rel. OD)
FLAG
FLAG
TUBA
[3MA] 10 mM
[MG132] 10 μM
[EHNA] 100 μM
TARDBPΔC

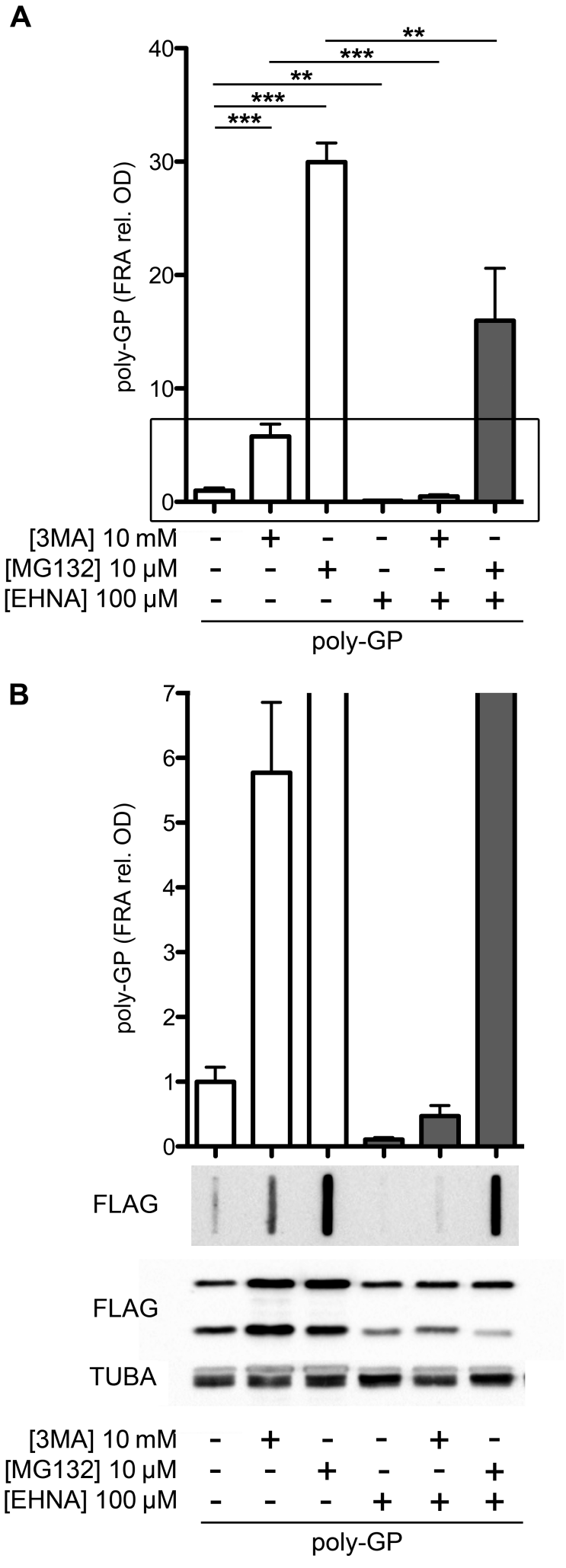
A
poly-GP (FRA rel. OD)
40
30
20
10
0
***
***
**
***
**
[3MA] 10 mM - + - - + -
[MG132] 10 µM - - + - - +
[EHNA] 100 µM - - - + + +
poly-GP
B
poly-GP (FRA rel. OD)
7
6
5
4
3
2
1
0
FLAG
FLAG
TUBA
[3MA] 10 mM - + - - + -
[MG132] 10 µM - - + - - +
[EHNA] 100 µM - - - + + +
poly-GP